PEOPLE'S DEMOCRATIC REPUBLIC OF ALGERIA MINISTRY OF HIGHER EDUCATION AND SCIENTIFIC RESEARCH

MOHAMED BOUDIAF UNIVERSITY - M'SILA

FACULTY OF TECHNOLOGY

DEPARTMENT : Electrical engineering

N° :

OPTION: Science of technology

SPECIALTY: Industrial maintenance

Final Study Dissertation In The Aim Of Obtaining a Master's Degree

Presendet by

ABDELATIF IBRAHIM

CHAICHE ALI

Title

Theoretical and Experimental Study of Magnetic Field Leakage Testing of Drill Pipes

Supported by the jury composed of:

Dr. DEFDAF MABROUK	**Université de M'sila**	**President**
Prof.BOUCHALA TARIK	**Université de M'sila**	**Advisor**
Prof.ZINE GHEMARI	**Université de M'sila**	**Examiner**
Mr. BELKHIRI KAMEL	**Université de M'sila**	**Co-Advisor**

Academic Year : 2024 /2025

Abstract

This study aims to analyze and use MFL technology as an effective tool in non-destructive testing (NDT) to detect defects such as cracks and corrosion in drill pipes, through 3D simulation and experimental studies. In fact, the comparison of the simulation results to experimental ones shows a good concordance. In addition, the simulation and experimental study make in evidence the effect of some electrical and mechanical parameters on defect detection sensitivity such as coils excitation density, its dimensions, scanning speed and defect orientation and dimensions. In context, we recall that many researchers had presented and validated some solution to compensate the effect of lift-off variation and acceleration velocity.

ملخص

للكشف (NDT) كأداة فعّالة في الاختبارات غير الإتلافية MFL تهدف هذه الدراسة إلى تحليل واستخدام تقنية عن عيوب مثل الشقوق والتآكل في أنابيب الحفر، وذلك من خلال محاكاة ثلاثية الأبعاد ودراسات تجريبية. في الواقع، تُظهر مقارنة نتائج المحاكاة بالنتائج التجريبية توافقًا جيدًا. كما تُثبت المحاكاة والدراسة التجريبية تأثير بعض المعلمات الكهربائية والميكانيكية على حساسية الكشف عن العيوب، مثل كثافة إثارة الملفات، وأبعادها، وسرعة المسح، واتجاه العيب وأبعاده. وفي هذا السياق، نذكر أن العديد من الباحثين قد قدموا وصادقوا على بعض الحلول لتعويض تأثير تغير الانطلاق وسرعة التسارع.

الإهداء

في المقام الأول، يجب أن أعرب عن□كري اللامحدود لله عز و جل، على تيسيره، من خلال منحنا الفرصة والشجاعة والصبر والطاقة الكافية لإنجاز وإكمال هذا المشروع.

ثانيا اود أن أعرب إمتناني العميق لعائلاتنا لدعمهم لنا طيلة أيام الدراسة

أخيرا نود أن نعرب عن خالص□كرنا وامتناننا لمعلمنا الدكتور **BOUCHALA TARIK** و **REZIGUI HOUSSEM EDDINE** لا□رافه و دعمه.

ولا ننسى لجنة التقييم الأستاذ السيد **DEFDAF MABROUK** والسيد**ZINE GHEMARI** لإهتمامهم بالعمل.

Contents

List of figures

List of tables

General Introduction

As critical components of drill strings, drill pipes are used to transmit torque and transport drilling fluids. During drilling operations, drill pipes withstand complex alternating stress loads, such as the pull, push, twist, and bend. In the meantime, drill pipes are also corroded by drilling fluids, which contain corrosive media such as dissolved O2, CO2, and H2S. As a result, cracks and corrosions easily develop in drill pipes, weakening the strength of drill pipes and even causing fracture failure [1]. Therefore, to avoid accidents and economic losses, according to the API (American Petroleum Institute) standard, drill pipes should be inspected by NDT (nondestructive testing) technologies before use [2].

Magnetic flux leakage (MFL) testing is an electromagnetic nondestructive testing (NDT) method with high efficiency and reliability. It has the ability to detect various types of defects such as cracks, corrosion, pitting, and cavity, and it is able to detect both surface and subsurface defects. Therefore, it has been widely used to ensure the integrity and safety of structures in the petrochemical, energy, manufacturing, and transportation industries.

The principle of MFL testing is based on the interaction between magnetic field and defects. The MFL testing device usually consists of a magnetizing unit, a sensing unit, a signal conditioning unit, an analog-to-digital converter (ADC), and a computer with signal displaying and analyzing software. So, magnetizing coils are able to magnetize the ferromagnetic specimen into saturation or near saturation. Due to the abrupt change in magnetic reluctance at the defects, the magnetic flux leaks into the nearby air. The perturbation of the magnetic field can be recorded by an array of magnetic field sensors and used to evaluate and quantify defects.

This work is constituted of three chapters:

- The **first chapter** is dedicated to basics of magnetic field leakage testing, modeling, applications and limitations.
-
- The **second chapter** consists of implementing the 3D model of electromagnetic inspection device in order to study the effect of the magnetization system characteristics on the concentrating field shape and amplitude. In addition to this we study the effect of the defect parameters and Lift-off on MFL signals.

Finally, the last chapter consists of conducting practical tests with an MFL inspection device available in the national drilling company ENAFOR.

1. Chapter I

1.1. INTRODUCTION

Magnetic flux leakage (MFL) technique is an electromagnetic NDE technique. MFL technique uses sensor for detection of leakage magnetic fields in comparison with the ferromagnetic particles/powders used in magnetic particle testing (MPT) [1,2]. The use of sensor enables incorporation of latest advances in field sensing devices towards enhanced detection as well as quantitative sizing of deep-surface (embedded) defects and this is a clear advantage over the MPT.

MFL technique is widely used in industry for assessing the quality and structural integrity of ferromagnetic components such as underground pipelines, oil-storage tank floors, rail- tracks, ropes etc. by way of detection of surface and sub-surface defects [3-5]. It is also used for automated testing of symmetric components such as steel rods, tubes, pipes and bars.

With the development of new sensor materials, digital devices and microelectronic systems, the capabilities and applications of the MFL technique have increased significantly in the last two decades. Further, numerical models,have enabled design of optimized MFL systems and sensors, besides better understanding of the phenomenon and the interactions. This paper gives a detailed overview of the state-of-art of the MFL technique and highlights the recent advances as well as future directions.

In this chapter we explain the working principal of the magnetic field leakage nondestructive testing, application, modeling of the electromagnetic phenomenon, the different magnetic field detection sensors, advantages and limitation.

1.2. PRINCIPLE

In MFL technique, the test object is uniformly magnetized, close to magnetic saturation. If any defect is present in the object, due to reduction in effective magnetic permeability and cross sectional area, magnetic flux lines leak out of the object surface around the defect as shown in Fig. 1. The leakage flux in three directions viz. B, (along the measurement surface and perpendicular to the length of defect), B, (along the measurement surface and parallel to the length of defect) and B, (perpendicular to the measurement surface) can be measured using magnetic field sensors and can be correlated with the shape and size of the defect responsible for the leakage flux. For regularly shaped defects, the tangential (B) and normal (B) components are usually measured.

Success of MFL testing depends on i) proper magnetization of the test object, ii) detection of leakage flux using a suitable sensor, iii) processing sensor response, and iv) interpretation of the test results for decision making. The test object can be magnetized using i) permanent magnets, ii) electromagnets such as yoke, or iii) by injecting electric current directly through the object. Permanent magnets are seldom preferred, as magnetization cannot be turned off when desired. This problem is absent with electromagnet and current injection methods [4]. In all the three magnetization methods, it is necessary to ensure that the magnetization is perpendicular to the expected orientation of defects such that maximum leakage field is produced at the object surface, for detection by the sensor. The intensity of leakage magnetic field depends on the method of magnetization.

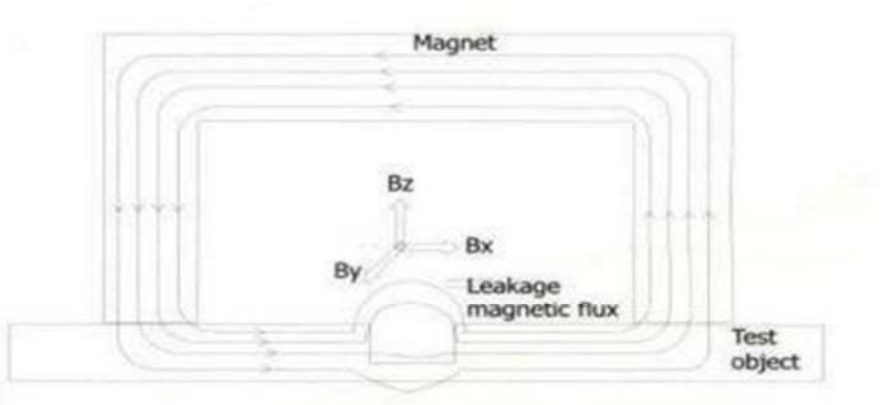

Figure 1: Principle of magnetic flux leakage technique.

such as magnetizing by permanent magnet, current flow or via magnetizing coils. When the magnetizing field is small, the magnetic flux lines are not able to come out of the defect region of the test object. On the other hand, the signature of leakage magnetic field may be masked by the surface noise, if magnetizing field is very high. Both active and residual magnetization methods are employed [5]. A study of the residual magnetization MFL signal can provide useful information about the size and shape of the defect. However, the leakage field due to residual magnetization is comparatively weak and requires sensitive detectors.

For MFL testing of components. magnetizing unit and sensor are scanned together as a single unit at constant velocity and the sensor response is recorded and interpreted continuously. Raster-scans are made using single sensor for imaging purpose while use of line-scan of array sensors is also not uncommon. The magnitude of MFL signal is strongly related to defect depth. The MFI. signal amplitude. increases almost linearly with the increase in defect depth when all other variables kept constant. Beside defect depth, the influence of defect width has to be taken into account for defect sizing. The MFL signal amplitude increases slightly with the defect width [6-7]. When the defect width is sufficiently large, the MFL signals become bloom. The defect length does not affect MFL signal amplitude much and the signal amplitude decreases slightly when defect length increases. In general, the length of the flux leakage field signal trace can be related to the length of the defect. The signal amplitude is larger for more gradual defects with the same volume of metal loss, and less for more sharp defects [8]. In addition, the length of the flux leakage field is less for more gradual defects.

Lift-off distance is an important parameter for detection and sizing of defects in MFL testing. Lift-off affects both the magnetization level and the signal shape. MFL signal amplitude decreases with increase in lift-off value (d) by a proportionality 1/d. When the lift-off value becomes larger, its influence on MFL amplitude decreases. In general,

constant and minimum possible lift-off over the volume of the object) is the is always preferred.

Stress variations in the test object that influence the magnetic permeability and changes in velocity of the MFL unit, produce disturbing MFL signals that create confusion during the interpretation and evaluation stages [9]. This demands the use of signal processing techniques.

1.3. MODELING

One of the most attractive features of MFL technique is mathematical simulation of leakage field from defect zone in a magnetized material. Simulation aids prediction and visualization of field/defect interaction and thus allows better insight and useful application of the MFL technique. MFL simulation is either based on analytical modeling technique or numerical modeling technique...

1.3.1. ANALYTICAL MODELING

In analytical modeling, defects are assumed as magnetic dipoles developed at the walls of the defect. The leakage flux signals are calculated from the dipole magnetic field of the magnetic dipoles. The analytical modeling has the advantages over numerical modeling as it offers exact closed form solution and is convenient for simple geometries. In the absence of free current, the magnetic field intensity HX) H(x) at any arbitrary point x is given by

$\mathbf{(x) = -\nabla\phi_m(x)}$ **…….. (1)**

Where the magnetic scalar potential (x) satisfies the following integral equation

$$\phi(\mathbf{r}) = \frac{1}{4\pi}\oint_S \frac{\mathbf{M}\cdot d\mathbf{S}}{|\mathbf{r}-\mathbf{r}'|} - \frac{1}{4\pi}\int_V \frac{\nabla'\cdot\mathbf{M}(\mathbf{r}')}{|\mathbf{r}-\mathbf{r}'|}\, dV' \quad \ldots\ldots\ldots\ldots (2)$$

where M is the magnetization (dipole moment per unit volume) of the magnetized object. The two terms on the right side of equation (2) corresponds to two distinct sources of magnetic leakage field associated with a defect. The first term (integral over the surface of object) is the induced surface magnetic charge density o=M.dS contributed due to the distribution of uncompensated magnetic poles on the defect surface. The second term (integral over the volume of the object) is the induced volume magnetic charge density
p=-V-M contributed due to variations in the permeability of the object near the defect.
Zatsepin and Scherbinin [10] pioneered the analytical modeling of 2-D field of surface breaking defects with approximating defects as point, line, plane and strip magnetic dipoles. They derived the expressions for normal and tangential components of leakage magnetic field due to a defect based on approximation of surface defects as lineardipoles. Later on, Shcherbinin and Pashagin [11-12] improved this model by considering three-dimensional defects with rectangular cross-sections and parallel sides. They also presented experimental evidence that the surface magnetic charge density on the defect walls is not uniform along the defect width. It is higher at the center of the walls than at the defect edges. Novikova and Miroshin [13] proposed that MFL fields are caused not only by surface magnetic charge on the defect walls, but also by volume magnetic charge close to the defect walls inside the bulk specimen. They approximated the volume magnetic charge for a 2-dimensiuonal rectangular cross-section defect by a line dipole close to the defect.
Based on the double dipole model, Förster [14] proposed the approximate equations for tangential (H_{1}) and normal (H) components of leakage field for a surface-breaking slot of a finite depth d in a linear isotropic medium magnetised by a uniform magnetic field H sigma' Using the idea of the Förster's dipole model and the image theory, Y. Zhang et al [15] derived expressions for the tangential (H .) and normal (H) components of leakage field for a rectangular defect (depth, d) located at a depth h below the surface of the material magnetised by a uniform magnetic field H as

$$H_x = -\frac{m_1(y+h)}{x^2+(y+h)^2} + \frac{m_2(y+h+d)}{x^2+(y+h+d)^2} \quad \ldots\ldots\ldots\ldots (3)$$

$$H_y = -\frac{m_1 x}{x^2+(y+h)^2} + \frac{m_2 x}{x^2+(y+h+d)^2} \quad \ldots\ldots\ldots\ldots (4)$$

Where

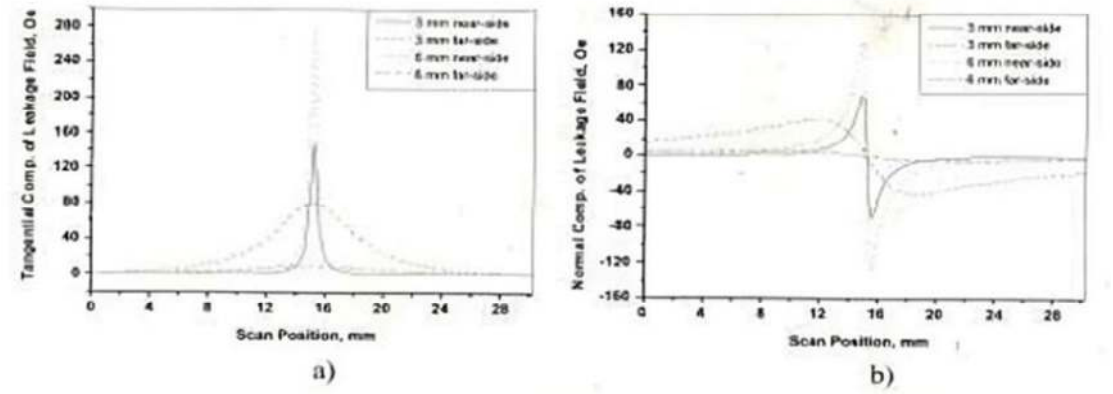

Figure 2 : Predicted a) tangential and b) normal components of MFL signals of near-side and far-side notches in a 2 mm ferromagnetic material

$$m_1 = \frac{H_0(2d+w)}{2\pi}\{1 - [(\frac{\mu-\mu_0}{\mu+\mu_0})^2(\frac{w}{4h})^2]\}^{-1} \text{ ..... (5)}$$

$$m_2 = \frac{H_0(2d+w)}{2\pi}\{1 - [(\frac{\mu-\mu_0}{\mu+\mu_0})^2(\frac{w}{2(h+2d)})^2]\}^{-1} \text{ ..... (6)}$$

The typical tangential and normal components of leakage fields computed using the above equations for near-side (only d) and far-side notches (d and h) are shown in Fig. 2.

Recently an analytical has been proposed model to account for variation of surface magnetic charge density for defect surfaces oblique to the direction of applied field. They predicted all orthogonal components of 3-dimensional MFL field of a surface breaking defect [16].

The analytical modeling approach has facilitated enhanced understanding of the MFL technique and prediction of MFL. signals from defects in simple geometries.

1.3.2. NUMERICAL MODELING

The use of numerical methods such as finite difference, finite element, boundary element, Hybrid, etc. gained popularity in MFL testing [17-23]. Compared to the analytical models, the finite element method has shown many advantages, including the processing of nonlinear problems and ability to model the irregular geometries found in actual defects. However, it requires intensive computer resources. Calculation of leakage fields was first attempted by Huang and Lord [18] using FE method and it was shown that the FE method provides the possibility of defect sizing from the leakage field profile.

NathanIda et al [21] realized a 3-D active leakage field model around a rectangular slot in a ferromagnetic bar. A detailed account of FE modeling is given elsewhere [23].

3D FEM was used to

- analyze the relation between defect parameters (length, width and depth) and MFL signals of surface defects.
- simulate the effect of complex corrosion on MFL signals.
- simulate the effects of different pit corner geometries on MFL signals.
- analyze the influence of air gap between the magnetizing yoke and specimen and also the specimen thickness on the detectability by MFL. Technique.
- analyse the changes in the shape and magnitude of the signal with the velocity of the axial as well as circumferential MFL systems.
- study the leakage fields from near-side and far-side defects in a 12 mm thick

carbon steel plate.

COMSOL 3.4 Multiphysics software package has been used for 3-D FE modeling. Typical magnetic flux density profiles of a near-side slot of 3.32 mm depth and a far-side slot located at 6.24 mm below the surface of a 12 mm thick carbon steel plate are shown in Fig. 3. The leakage magnetic field for far-side slot is weaker than that of the near-side slot and their detectability requires the use of high sensitive sensors such as GMR sensors [24].

1.4. SENSORS

Various magnetic field detection sensors such as pick-up coils, Hall sensors, magnetodiodes, fluxgates, anisotropic magnetoresistance (AMR) and Giant-magneto-resistive (GMR) sensors are commonly used in MFL, technique [25, 26]. Table 1 compares the performance of various sensors used.

1.4.1. PICK-UP COIL

Pick-up coils consist of some turns of copper wire wrapped around a core. They measure the change in magnetic field due to the presence of defects in the object. They have the advantages of being cheap, high flexibility in sensor configuration and no saturation even at quite large excitation levels. However, they are less sensitive.

1.4.2. HALL SENSOR

Hall sensor is the most commonly used flux leakage sensors. It works on the principle of Hall effect and measures the normal component of the magnetic field. A typical Hall device consists of indium arsenide, indium antimony, gallium arsenide or silicon. It has the advantages of high linearity, small size, inexpensive, room temperature operation and fabrication of sensor arrays. However, they suffer from limited sensitivity and large offset. Recently, micro-Hall sensors are also used in MFL NDE applications due to their high sensitivity and wide linear response [27].

Figure 3 : FE model predicted array contour plots for a a) 3.32 mm deep near-side notch and b) 3.32 mm deep far-side notch located at 6.24 mm below the surface.

Tableau 1 : coparison of sensors in MFL technique.

Sensor type	*Physical principle*	*Detectable field range (T)*	*Sensitivity (V/T)*	*Response time*	*Sensor head size*	*Power consumption*
Pick-up coil	Faraday EMI	10^{-4}- 10^{3}	0.25	1kHz	2-10 mm	1W
Hall	Hall effect	10^{-6}- 10^{2}	0.65	1 MHz	10-100 im	10 mW
Fluxgate	Faraday EMI	10^{-10}- 10^{-2}	3.2	5 kHz	10 -20 mm	1W
Magneto-diode	Magneto-resistance	10^{-5}- 10^{0}	2.7	1MHz	10-100 im	10 mW
AMR	Magneto-resistance	10^{-5}- 10^{0}	2.5	1 MHz	10-100 im	10 mW
GMR	GMR effect	10^{-12}- 10^{-2}	120	1 MHz	10-100 im	10 mW

1.4.3. MAGNETODIODES

A magnetodiode consists of a small thin rectangular plate of an intrinsic semiconductor doped

to make n-type at one end and p-type to other end. Indium arsenide is generally used as magnetodiode. It works based on magnetoresistance in which there is increase in electrical resistance with the square of magnetic field applied normal to the electric current. The sensitivity of magnetodiode is greater than Hall sensor, however, it fails at high magnetic fields due to saturation [8].

1.4.4. FLUXGATE SENSORS

It consists of a ferromagnetic core upon which two coils are wound: the primary (excitation) coil, and the secondary (pick-up) coil. Provided the ferromagnetic core is not saturated, it offers a low magnetic resistance path to the flux lines of the external field. When the core saturates the magnetic resistance of the core increases and the excess magnetic flux lines are forced out of the core. The fluxgate sensors undergo reduced sensitivity when its size is minimized and incompatibility with planar technologies being utilized within the microelectronics field.

1.4.5. AMR SENSORS

Anisotropic magnetoresistance (AMR) occurs in ferromagnetic materials depending on the angle between the electric current and the magnetization direction. The application of an external magnetic field will rotate the magnetization with a resulting change in resistance. The MR ratio for AMR materials is typically a few percent. Integrated AMR sensors are commercially available. They have the advantage of less noise as compared to thin-film multilayers of giant magneto-resistance (GMR) sensors.

1.4.6. GMR SENSORS

GMR sensor is constructed from a few nm thick multilayer films such as Fe/Cr/Fe, Co/Cu/Co, etc. with ferromagnetic layers being separated by non-magnetic layers. The sensors rely on the GMR effect in which there takes place an enormous change in electrical resistance to an applied magnetic field due to spin dependent scattering of electrons [25]. GMR sensors show high sensitivity with low magnetic field and high spatial resolution [28]. They can be integrated as arrays to perform rapid scanning of surfaces. They suffer from hysteresis effect and low saturation field. Authors used an array of eight GMR sensors with suitable software in Lab view for data acquisition from eight GMR sensors, processing, and forming on-line MFL image of defects. The sensor array could image and detect defects as shallow as 0.5 mm deep in 12 mm thick carbon steel plate and also defects 6 mm below the surface.

1.4.7. SELECTION OF SENSOR

Sensor choice decides the effectiveness of the MFL technique. For example, Hall sensors are wanted to identify deep surface defects in high magnetic field conditions and GMR sensors are wanted to identify deep buried defects, as long as sensor saturation is considered. The MFL signal pattern changes with sensor types. For example, tangential component of MFL signal with pick-up coils is different from that measured with the solid state sensors. This is due to the fact that pick-up coils measure the change in the magnetic field while the solid state sensors measure the magnetic field. Sensor size is an important factor to detect defects and find their sizes. Leakage fields are incorporated over the active region of the sensor, which reduces the detectability of short cracks. Coil sensors are normally robust, although not having good sensitivity. Hall sensors have enormous dynamic range (linear) as opposed to GMR sensors. Hall sensor is most sensitive along the direction perpendicular to the plane of the chip whereas GMR sensor is most sensitive along the direction parallel to the plane of the chip. Sensor is selected based on the expected location and type of defects and the leakage fields from them. In most applications, the use of two sensors (coil and Hall or GMR and Hall) that

can simultaneously solve the sensitivity and the saturation issues is preferred. Array sensors with imaging capabilities are emerging in this regard. For instance, a magnetic camera of the scan type, utilizing two linearly integrated 64 element Hall sensor arrays (LIHaS) on a wafer, and a miniature yoke-type magnetizer can detect tiny cracks on express train wheels with high-speed and high spatial resolution [29].

1.5. CAPABILITIES AND APPLICATIONS

Like other NDT techniques, MFL technique has definite capabilities and popular industrial applications. Sensors Clearly enhance the capability of the MFL technique by incorporating advances in magnetic materials, electronic devices, and measurement techniques.

1.5.1. CAPABILITIES

The MFL technique is capable of detecting and sizing surface and subsurface defects in ferromagnetic objects [4-8]. A few clearly established capabilities of the MFL technique include:

- Detection of corrosion, cracks, gouges, and dents in pipelines and storage tank floors
- Detection of localized flaws and loss of metallic cross-sectional area in wire ropes
- High sensitivity for detecting small surface cracks in components without removal of paint or rust
- Automatic MFL testing of axi-symmetric components in the production line
- NDT of hot objects.

1.5.2. Applications

The MFL testing is extensively used for in-service inspection of engineering components. It is important to know that about 80% of pipeline inspection is carried out using the MFL technique. The MFL technique has been applied to post-process inspection of tailor-welded blanks (TWBs) [30]. A few important and popular applications of the MFL technique are discussed in this subsection.

1.5.2.1. On-line inspection of gas-transmission pipelines

MFL is the oldest and most commonly used in-line inspection technique for the identification of metal-loss regions in gas-transmission pipelines.

As much as 80% of pipeline inspection is carried out using the MFL technique. MFL can identify metal loss due to corrosion and, in certain instances, gouging that occurred in gas-pipelines. PIG (Pipe Inspection Gauge) is commonly used for inspecting the structural integrity and damage of gas-pipelines [4]. A diagram of a typical PIG for gas pipeline inspection is shown in Fig 4. The PIG is propelled within the pipe by the pressure of natural gas. The strong permanent magnet in the PIG near-saturates the pipe wall and an array of Hall sensors clamped around the pipe circumference measure the leakage flux from defects. The sensan response is measured and stored in an on-board computer and subsequently analyzed by advanced signal processing methods. It is possible to image defects and exactly identify the position, for possible repair. Localized stress in pipe reduces the MFL, signal amplitude, however, to a different extent in active and residual methods. The residual flux pattern has magnetic polarity exactly opposite to that of active flux pattern. The residual scans have the potential to reveal the size and shape of anomalous defects.

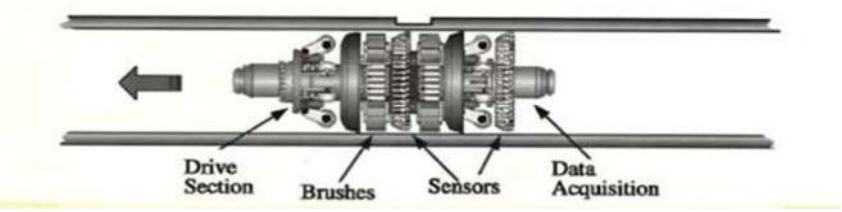

Figure 4: MFL PIG inspection of gaz pipelines.

1.5.2.2. Testing flaws in oil storage tank bottom floors

MFL technique is being widely applied in detecting defects and corrosion on the floor of storage tanks. Kasai et al [3] used Hall probe to measure tangential and normal components of leakage fields from an array of flat-bottomed holes and rectangular grooves of various widths and depths in 12 mm and 22 mm thick carbon steel plates. The leakage magnetic profile is found to depend on the ratio of flaw depth to width. Using the MFL method, it is possible to measure the depth of far-side flaw or remaining thickness of the metal loss area in case of constant lift-off. Liu et al [31] reported that different areas of tank floors do not affect the testing sensitivity, if the thickness is the same. Climatic conditions, surface cleanliness and condition need to be considered, along with personnel training. However, MFL technique is a rapid, efficient, and effective technique for assessment of the condition of floor corrosion and tank bottom. Automated steerable motorized MFL systems are also being used for above ground storage tanks for detecting metal loss due to corrosion.

1.5.2.3. Inspection of Wire Ropes

Wire ropes are generally deteriorated in the form of local flaw (LF) and metallic cross-sectional area loss (LMA). Local flaws are those internal and external discontinuities such as broken wires and corrosion. Broken wires are caused by fatigue, inter-strand nicking and martensitic embrittlement. Metallic cross-sectional area loss is caused by external or internal corrosion, abrasion and wear.

A number of techniques using different types of sensors and magnetizing devices have been employed for defect detection in wire ropes reliably [32-33]. Jomdecha et al. [33] employed printed circuit-shaped coils in series as field sensors and solenoid as magnetizing unit for inspection of wire rope and demonstrated the detection of 2 mm deep surface defects in a wire rope of 38 mm diameter. Kalwa et al. [34] developed an MFL system with magnetic concentrators and Hall and coil sensors for enhancing the detection sensitivity of steel rope defects. They suggested measuring tangential component.

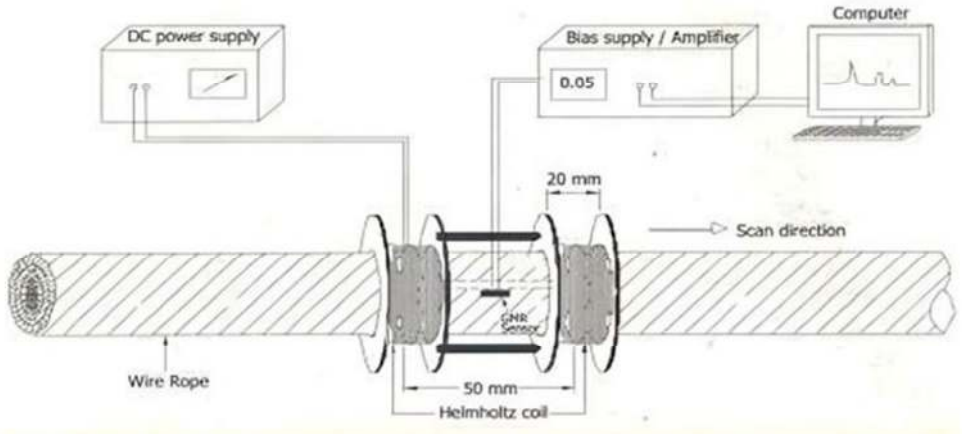

Figure 5: GMR sensor based MFL testing set-up.

Figure 6 : GMR array sensor probe with saddle tybe coil developed for inspection of steel track ropes.

is more versatile than normal component for detection of multiple defects in wire ropes.
Recently, authors developed GMR sensor based MFL technique for inspection of steel track rope of 64 mm diameter, used for transportation of coal. The track rope has 8 layers of stranded wires of different diameters [35]. The MFL technique used Helmholtz coil as well as saddle type coils for magnetizat

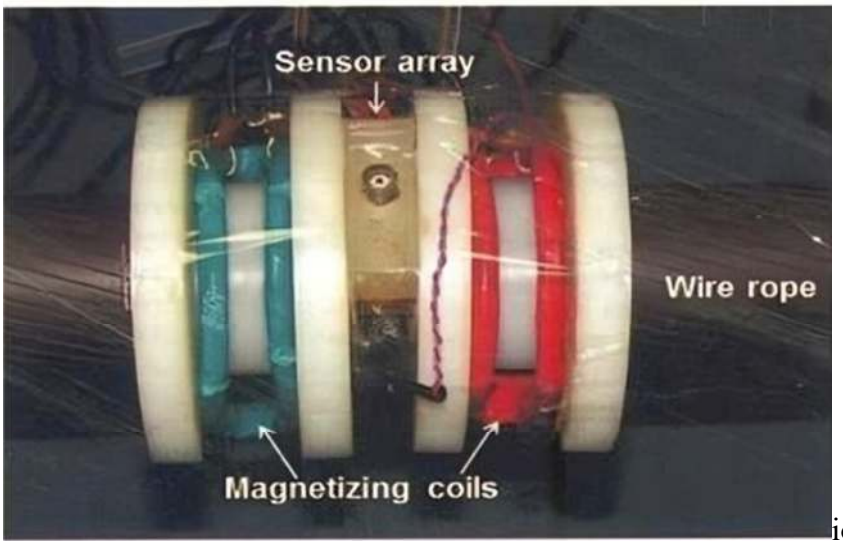

ion purpose. The typical signals of the artificial LFs. (circumferential EDM notches) of different depths (length. 5.5 mm, width, 2.0 mm) in the track rope are shown in Fig. 5. The technique is able to readily detect both LF and LMA defects in the rope. Typical GMR array sensor probe with saddle type coil developed is shown in Fig 6.

1.5.2.4. Testing of flaws in ferromagnetic tubes and rods

Many MFL devices have been developed by Forster for the automatic testing of tubes and rods of diameters ranging from 10 to more than 500 mm.
One device, called "rotomat", enables the tube to pass through a rotating magnetizing yoke for detection of longitudinal defects in the tube wall [7].
Authors developed GMR based MFL technique for detection of localized defects in steam generator tubes of Prototype Fast Breeder Reactor (PFBR). The performance of the technique was evaluated by measuring the axial component of the leakage fields from outer side circumferential defects [36]. It was found that the technique is not influenced by the presence of Inconel support structures and sodium deposits in defects.

1.5.2.5. Detection of defects in steel plates

For MFL testing of ferromagnetic steel plates, yoke based magnetization is employed. In plates covered with paints. Inspection is possible without removing paint. It is essential to optimize the magnetizing current and sensor location. Finite element modeling is helpful in this regard. Authors used an experimental set-up (Fig. 7) consisting of an electromagnetic yoke, GMR sensor, X-Y scanner, amplifier and personal computer for the MFL measurements on a 12 mm thick carbon steel plate. The measured. B, and B, components signals for far-side notches located at different depths in carbon steel plates are shown in Figs. 8(a) and (b) respectively. As can be seen, the signal amplitude is found to decrease with increase in the notch location below the surface. The MFL. Signal response from the farthest far-side notch located at 11.07 mm below the surface is well above the background signal. B amplitude is found to be higher than B, amplitude for all the notches.

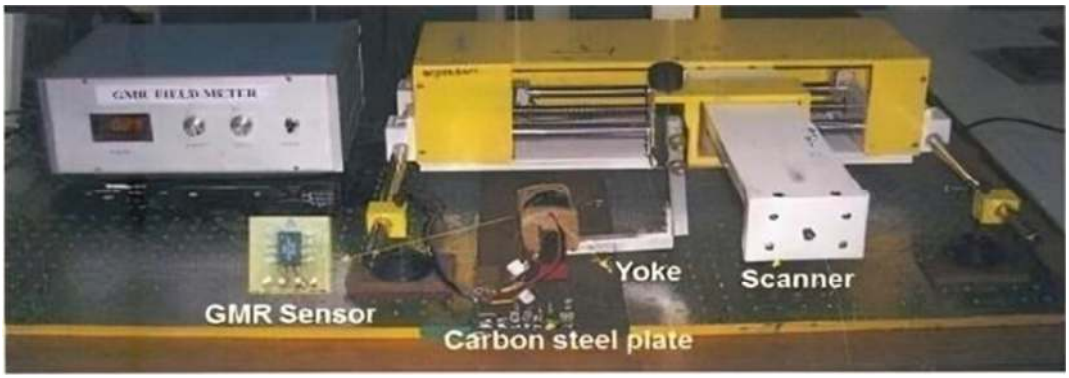

Figure 7: Experimental set-up for MFL measurements in carbon steel plates.

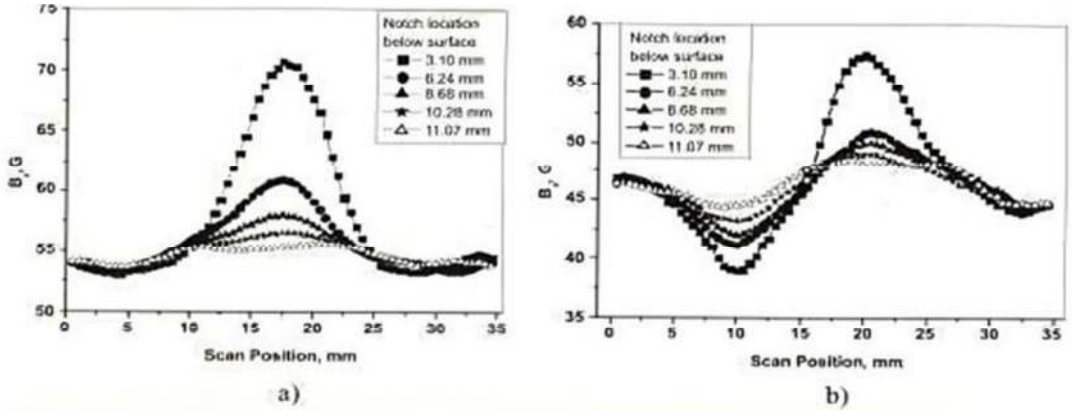

Figure 8: Measured a) B, and b)B, component signals for far-side notches located at different depths below the surface in carbon steel plates.

MFL signal analysis of neighboring defects is important. The signals are a manifestation of the interacting magnetic dipole moments of the individual defects. Researchers carried out 3D-FE modelling in order to study such interacting defects with a view to understanding the nature of the MFL signals. Tangential (B) and normal (B) components of MFL signals from defects with different dimensions and separation in a 14 mm thick carbon steel plate have been simulated. The intensity of the MFL signal depends on the depths of interacting defects as well as on their separation. The amplitude of MFL signal of the bigger defect decreases with the depth increase of the interacting defect for the same defect-to-defect distance. The effect of inclined defects (inclination changed by 0°. 15°, 30°, and 45°) on MFL signals has also been studied. Model predictions have been experimentally validated for some chosen cases. MFL signal parameters such as peak amplitudes and B-B, locus have been extracted to differentiate between interacting and non-interacting defects. To differentiate between interacting defects and non-interacting defects, parameters such as ratio of peak amplitudes, area and width of inner lobe in the B-B, locus have been extracted from the MFL. signals. Among the various features, ratio of the peak amplitudes of MFL. signals of slots has been a more successful parameter in classifying interacting defects [28]. The use of such parameters will enable fast detection and effective characterisation of plate geometry defects.

1.5.3. EVALUATION OF STRESSES AND PLASTIC DEFORMATION

Stresses and residual stresses influence the MFL signals. Applied and residual stresses affect the magnetization curve, which in turn, reduce flux leakage signal amplitude. Similarly, plastic strains affect the leakage flux. These effects are largest in high-pressure lines and where there is significant secondary loading. This can be significant when sizing of defects in or near dents and attachments are demanded [37]. Masatoshi Kuroda et al [9] studied the relationship between the leakage magnetic flux and the residual stress measured by the X-

ray diffraction method. The amount of plastic deformations accumulated in the various steel (plate type pressure vessel steel of A533B, austenitic stainless steel of SUS304 and low carbon steel of S25C) specimens was estimated by processing the data of the leakage magnetic flux at each point obtained in the measurement. It was shown that the MFL. technique is promising to quantify the residual stress and the amount of the plastic deformation in iron-based materials. Clapham et al [38] studied the damage in the dents of plate samples. They found that there is increase in the magnetic permeability in the tensile stress direction. Conversely, an applied compression will increase the magnetic permeability in a direction transverse to the stress axis. They showed that MFL signal is not sensitive to plastic deformation. MFL technique is useful for detection and quantification of mechanical damage [39].

1.6. STANDARDS

There are a number of standards that exist for non-destructive testing or inspection of ferromagnetic parts using MFL technique. The standard practice used for MFL testing of ferromagnetic steel tubular products is given in ASTM E 570-97. It gives the application and standardization of equipment for steel tubular product transverse and longitudinal discontinuity detection through seamless and welded tubing with outer diameters 12.7 mm to 610 mm. ASTM E 1571-01 addresses the use and standardization of the utilization of instruments incorporating the electromagnetic, the magnetic flux. and the magnetic flux leakage testing technique to detect LFS and LMAs in ferromagnetic wire rope products up to a diameter of 63.5 mm. ISO 10893-3 Nondestructive testing of steel tubes Part 3 deals with 'automated full peripheral flux leakage testing of seamless and welded (except submerged are welded) ferromagnetic steel tubes for the detection of longitudinal and/or transverse imperfections. There is IS 11655:1986 by Bureau of Indian Standards on 'Procedure for stray flux testing of ferromagnetic seamless steel tubular products. International efforts are being made to adopt the ISO standards".

1.7. LIMITATIONS AND ISSUES

MFL technique suffers from the following drawbacks:

1. It is necessary to ensure that the magnetization is perpendicular to the expected orientation of defects so as to get maximum leakage field at the object surface.
2. MFL technique is applicable only for ferromagnetic materials.
3. It is a semi-volumetric NDE technique.
4. MFL signals are influenced by changes in stress and velocity, as a result, skill is required for data interpretation or application of signal processing techniques
5. It is necessary to measure both normal and tangential components for defect sizing.
6. Need for component demagnetization, if the component operating temperature doesn't exceed the Curie temperature

The MFL. signals depend on many factors including the defect geometry. sensor size and orientation, magnetizing circuit, and of course the sample's magnetic properties. MFL, response is also affected by the sensor lift-off from the test object [4]. Velocity of the inspection tool induces eddy currents in the test object which affect the leakage field. The impact of speed on MFL signal includes not just its form but also its measured amplitude. Amplitude of the MFL signal increases with increase in inspection speed. These have their maximum impacts at low to moderate magnetization levels and at shallow flaws. The lift-off and velocity variation disturbances can be reduced through digital signal processing.

1.8. Factor influencing MFL signal

Various factors affect the inspection signal during MFL testing. This section highlights some of the major factors such as defect size, defect orientation, liftoff, magnetization strength, stress, and scanning velocity.

1.8.1. Dimensions and Orientation of Defects

$$\sigma_m = \frac{1}{2\pi} \cdot \frac{\frac{b}{a}+1}{\frac{b}{a}+1(\frac{1}{\mu})} \cdot F_{nl} \cdot H_a$$

where F_{nl} is the non-linear factor, and Ha is the applied field. We can look into the influence of the defect dimensions through Equations (4)–(7). With the dimensions corresponding to the Figure 3b defect, the magnetic field above the center of the defect (y = 1 and z = 0) was extracted, and results are shown in Figure :

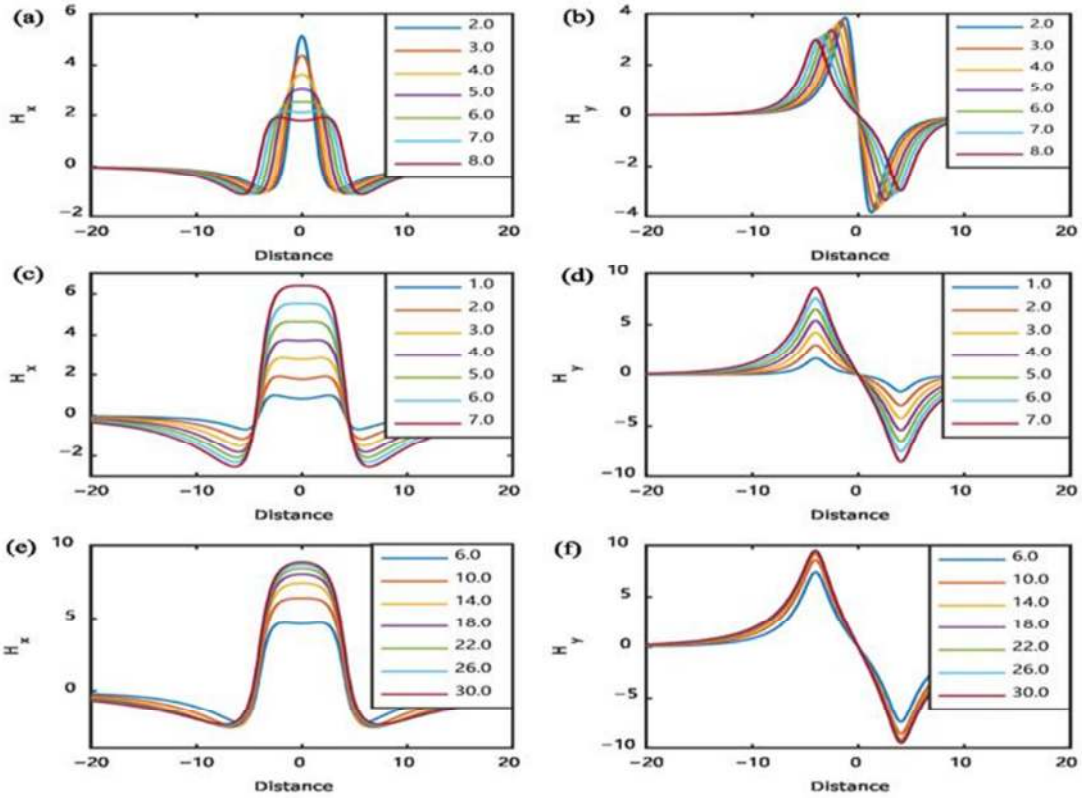

Figure 9: Influences of defect dimensions on MFL signal: (a) change in Hx with defect width; (b) change in Hy with defect width; (c) change in Hx with defect depth; (d) change in Hy with defect depth; (e) change in Hx with defect length; (f) change in Hy.

Conventionally, researchers and engineers working in MFL have considered that the orientation defect should be perpendicular to the magnetizing field for a prominent MFL field to be generated.

Sun and Song questioned the traditional viewpoint and have studied MFL signals for defects parallel to the magnetization field [55-56] . It was found that cracks parallel to the magnetization can indeed be detected, although with very low amplitude. Wu went further to study the variation of the amplitude of the MFL signal with the angle between the defect and the magnetization field [57] , and the results are displayed in Figure:

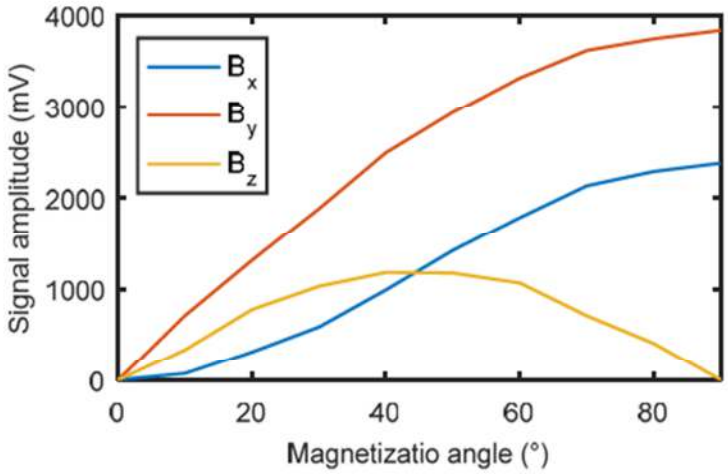

Figure 10: Influence of the angle between magnetization and defect on MFL signal.

$$H_x(x,y,z)=\frac{\sigma_m}{4\pi}\left(\arctan\frac{(y+b)(z+c)}{(x+a)[(x+a)^2+(y+b)^2+(z+c)^2]^{1/2}}-\arctan\frac{y(z+c)}{(x+a)[(x+a)^2+y^2+(z+c)^2]^{1/2}}\right.$$
$$-\arctan\frac{(y+b)(z-c)}{(x+a)[(x+a)^2+(y+b)^2+(z-c)^2]^{1/2}}+\arctan\frac{y(z-c)}{(x+a)[(x+a)^2+y^2+(z-c)^2]^{1/2}}$$
$$-\arctan\frac{(y+b)(z+c)}{(x-a)[(x-a)^2+(y+b)^2+(z+c)^2]^{1/2}}+\arctan\frac{y(z+c)}{(x-a)[(x-a)^2+y^2+(z+c)^2]^{1/2}}$$
$$\left.+\arctan\frac{(y+b)(z-c)}{(x-a)[(x-a)^2+(y+b)^2+(z-c)^2]^{1/2}}-\arctan\frac{y(z-c)}{(x-a)[(x-a)^2+y^2+(z-c)^2]^{1/2}}\right) \quad (4)$$

$$H_y(x,y,z)=\frac{\sigma_m}{4\pi}\left[\ln\left(\frac{z+c+[(x+a)^2+y^2+(z+c)^2]^{1/2}}{z-c+[(x+a)^2+y^2+(z-c)^2]^{1/2}}\times\frac{z-c+[(x+a)^2+(y+b)^2+(z-c)^2]^{1/2}}{z+c+[(x+a)^2+(y+b)^2+(z+c)^2]^{1/2}}\right)\right.$$
$$\left.-\ln\left(\frac{z+c+[(x-a)^2+y^2+(z+c)^2]^{1/2}}{z-c+[(x-a)^2+y^2+(z-c)^2]^{1/2}}\times\frac{z-c+[(x-a)^2+(y+b)^2+(z-c)^2]^{1/2}}{z+c+[(x-a)^2+(y+b)^2+(z+c)^2]^{1/2}}\right)\right] \quad (5)$$

$$H_z(x,y,z)=\frac{\sigma_m}{4\pi}\left[\ln\left(\frac{y+b+[(x+a)^2+(y+b)^2+(z-c)^2]^{1/2}}{y+[(x+a)^2+y^2+(z-c)^2]^{1/2}}\times\frac{y+[(x+a)^2+y^2+(z+c)^2]^{1/2}}{y+b+[(x+a)^2+(y+b)^2+(z+c)^2]^{1/2}}\right)\right.$$
$$\left.-\ln\left(\frac{y+b+[(x-a)^2+(y+b)^2+(z-c)^2]^{1/2}}{y+[(x-a)^2+y^2+(z-c)^2]^{1/2}}\times\frac{y+[(x-a)^2+y^2+(z+c)^2]^{1/2}}{y+b+[(x-a)^2+(y+b)^2+(z+c)^2]^{1/2}}\right)\right] \quad (6)$$

Also, the scanning direction of the sensors influences the MFL signal, and Wu studied[57] it again This phenomenon may also be explained by extracting the magnetic field along various directions using Equations (4)–(6). For a defect with sizes a = 1, b = 2, and c = 10, Figure displays how the MFL signal varies with the scanning direction.

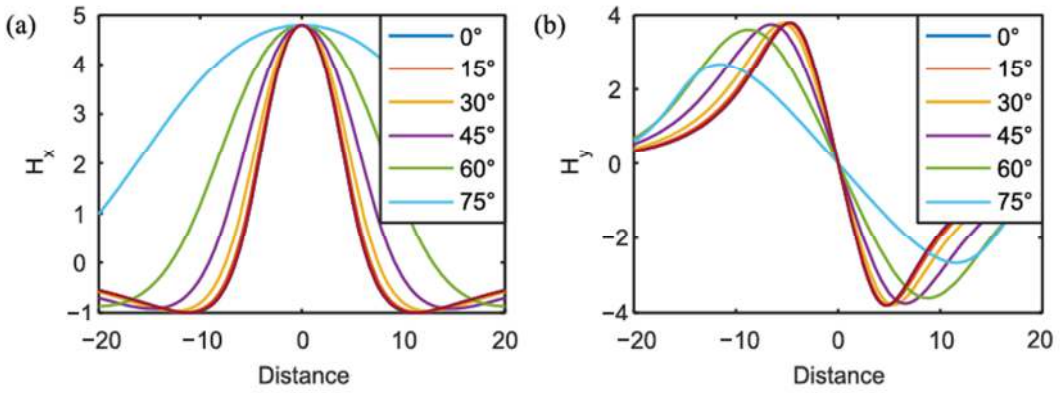

Figure 11: Influence of scanning angle on MFL signal: (a) change in Hx with scanning angle; (b) change in Hy with scanning angle.

1.8.2. Liftoff Effect

The MFL signal depends entirely on the liftoff distance [58-59] between the probe and the specimen Figure 12 presents an example of the liftoff effect through signal reduction at:

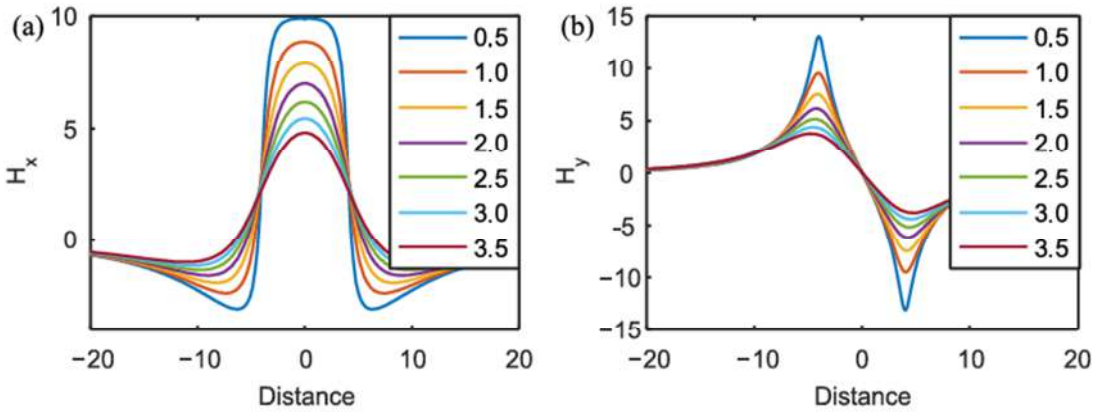

Figure 12: Influence of liftoff on MFL signal: (a) change in Hx with liftoff; (b) change in Hy with liftoff.

The change in liftoff during scanning significantly influences the testing signal. Thus, many researchers have attempted to reduce the liftoff effect. Jia used a filtering method to suppress liftoff interference [60] ; Wu proposed a liftoff tolerant sensor by inserting ferrite into the sensing coil [61] ; Peng introduced an exponential function compensation for liftoff correction [62] ; Wang linearized the liftoff effect by applying Fourier transform[63].

1.8.3. Magnetization Strength and Material Property

Usually, a strong magnetization is required to saturate the ferromagnetic material to obtain a good MFL signal. However, the MFL signal does not always increase with mag-netization strength. Many researchers have found that the MFL signal initially increases with the magnetizing current and starts to decrease after a certain point[64-65] , as shown in Figure 13. Sun explained this phenomenon with the magnetic compression effect [66] , which states that the large background field caused by strong magnetization suppresses the leakage of the magnetic field from defects. Later, he proposed a new MFL principle based on near-zero background magnetic field [67] , in which magnetic shielding is used. to collect a strong background field.
Since the magnetization of the material is also based on the material property, the MFL signal is also dependent on the B-H curve of the ferromagnetic materials. Katoh ap-proximated the B-H curve with two lines and studied this influence[68].

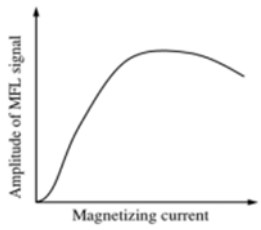

Figure 13: Influence of magnetizing current on MFL signal.

1.8.4. Velocity Effect

In pipeline inspection, the MFL device is propelled by the gas and oil inside the pipe. The device usually travels several meters per second. Due to the relatively motion between the magnetizer and the pipe, eddy currents are induced in the pipe wall. The mo-tion-induced eddy current density is:

$$\mathbf{J} = \sigma \mathbf{v} \times \mathbf{B}$$

The eddy currents generate a secondary magnetic field according to the Biot-Savart law. Thus, the magnetization status of the pipe and corresponding MFL signal will be affected at high testing speeds. The problem is governed by Maxwell's equations consid-ering the velocity term:

$$\nabla^2 \mathbf{B} - \mu\sigma \frac{\partial \mathbf{B}}{\partial t} - \mu\sigma(\mathbf{v} \cdot \nabla)\mathbf{B} = 0$$

Many researchers have studied the velocity effect of finite element simulation. For the yoke-type magnetizer, the eddy currents are induced in the region beneath the poles [69-71], and the magnetic field is perturbed [72]. A comparison between the distributions of the eddy current and magnetic field at different speeds is shown in Figure 14.

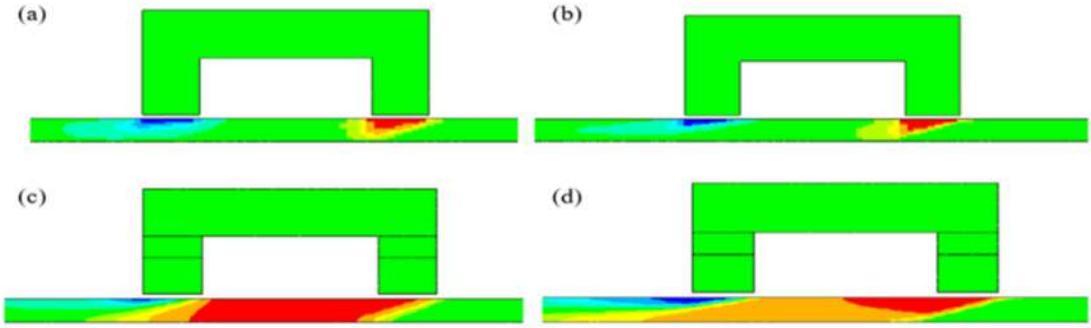

Figure 14: Distribution of motion-induced eddy current and magnetic field: (a) eddy current at 0.5 m/s; (b) eddy current at 2 m/s; (c) magnetic field at 0.5 m/s; (d) magnetic field at 2 m/s.

Recently, B. Feng found an analytical solution to Equation (9) and further obtained the expression of the motion-induced eddy current under a pole of the magnetizer [73] :

$$C_x^{III} = -\frac{2j\mu I k'(k'+k)\, e^{-ky'}\, k^* d \sin(ka)}{e^{k^* d}(k'+k)^2 - e^{-k^* d}(k'-k)^2}$$

$$D_x^{III} = \frac{2j\mu I k'(k'-k)\, e^{-ky'}\, k^* d \sin(ka)}{e^{k^* d}(k'+k)^2 - e^{-k^* d}(k'-k)^2}$$

$$C_y^{III} = -\frac{2\mu I k(k'+k)\, e^{-ky'}\, k^* d \sin(ka)}{e^{k^* d}(k'+k)^2 - e^{-k^* d}(k'-k)^2}$$

$$D_y^{III} = -\frac{2\mu I k(k'-k)\, e^{-ky'}\, k^* d \sin(ka)}{e^{k^* d}(k'+k)^2 - e^{-k^* d}(k'-k)^2}$$

With the analytical solution of the MIEC, the tail effect and tilt angle of the MIFC at different moving speeds are also analyzed . The encircling coil-type magnetizer is more commonly used in the manufacturing line for the inspection of steel pipes. As the production speed increases, there is also a need for high-speed testing. For the encircling coil-type magnetizer, the motion-induced eddy currents are mainly focused on the edge of the magnetizing coil [74-75] . Wu also studied the distribution of eddy current in circumferential-type MFL testing [76] .

The influence of the velocity on the MFL signal has also been extensively studied. There are changes in both the signal baseline and signal amplitude, and the signal shape is also distorted [77-78]. The change in MFL signal amplitude with velocity has been re-ported in many previous studies, some have reported that the signal amplitude decreases with the increase in velocity [70-74] . However, further detailed analyzes by Pullen showed that when there is insufficient flux saturating the specimen, the MFL signal for far-side defects decreases with scanning speed, while the signal for near-side defects increases with the speed [79-80] . Zhang further found that the influence of the velocity also depends on the sensor position [81] . In order to reduce the velocity impact, Usarek studied the change in the magnetic field with velocity and found that both tangential and normal components of the magnetic field increase with velocity linearly and used an empirical fitting equation to compensate for the MFL signal[82].

Based on the studies of the velocity effect in MFL testing, many researchers have at-tempted to use the velocity-induced field for testing. Antipov used an induced tail mag-netic field to test rails at high-speed [83] . B. Feng, T. Rocha, and F. Yuan all studied the motion-induced eddy current testing method and used magnetic field sensors to pick up the defect signals [73,84-85]. Researchers from Technische Universität Ilmenau proposed a new Lorentz force NDT method for conductive specimens, which is also based on mo-tion-induced eddy current[86-87].

1.8.5. Other Effects

In MFL testing, there are also other factors that influence the MFL signal, such as stress, surface roughness, corrosion coverage, and probe gesture. Kasai studied the MFL testing signal for samples covered by corrosion (iron oxides) and showed that the MFL signal decreased with increasing iron oxide ratio [88] . Long studied the influence of ges-ture probes on MFL signal and proposed a dual magnetic sensor model to compensate for the change in probe gesture **[**89**].**

The stress effect has been studied by many researchers [90-95] . The properties of fer-romagnetic materials change with the loading stress due to the magneto-mechanical cou-pling, thus the MFL signal also changes with the stress. Y. Wang proposed a multi-physics simulation model to study the change in MFL signal with stress and showed that the peak-to-peak amplitude of the normalized MFL. signal decreases with an increase in stress [90]. Mandal showed that the circumferential bending stress changes the magnetic easy axis of the pipe and thus reduces the MFL signal . Y. Wang also studied the stress-dependent MFL signals in Q235 steel plates . Timoshenko's theory and the J-A model were com-bined to calculate the stress-dependent distribution of magnetization, then a modified magnetic dipole model considering the stress dependence was proposed. With the pro-posed model, Wang showed that the MFL. signal increases with the increase in stress in the Q235 steel plate. Gao also observed a similar effect in the testing of steel wire ropes [93]. Later, Shi showed that the change in the MFL signal behaves differently in the elastic and plastic deformation stage [94].

For the testing of micro-cracks, the influences of surface roughness cannot be ig-nored. Deng considered the rough surface as concave and convex defects and showed that a rough surface introduces background noise to the MFL signal and reduces the signal-to-noise ratio (SNR)[96]. Yang also studied the effect of surface roughness on the SNR[97] of MFL signals and proposed the use of a magnetic medium to improve the SNR . In another study, B.P.C. Rao proposed the use of an Eigen vector-based

approach to suppress the noise caused by non-linear permeability, surface roughness, stresses, and liftoff vari-ations in MFL images[94]. Since the surface roughness influences the MFL signal, the MFL signal can be used in turn to represent the surface roughness. Li proposed to use the MFL signal and its spatial Fourier spectrum to measure surface roughness[99].

1.9. Conclusion

In this chapter, a comprehensive review of the MFL technology has been presented. So, the objective is to understand the principle of MFL nondestructive testing, application and the technological aspect of this method and the factors affecting the inspection results. We recall that the next chapter will be essentially dedicated for the numerical simulation of the MFL inspection of drill pipes.

2. Chapter II

2.1. Introduction

As critical components of drill strings, drill pipes are used to transmit torque and transport drilling fluids. During drilling operations, drill pipes withstand complex alternating stress loads, such as the pull, push, twist, and bend. In the meantime, drill pipes are also corroded by drilling fluids, which contain corrosive media such as dissolved O2, CO2, and H2S. As a result, cracks and corrosions easily develop in drill pipes, weakening the strength of drill pipes and even causing fracture failure [100]. Therefore, to avoid accidents and economic losses, according to the API (American Petroleum Institute) standard, drill pipes should be inspected by NDT (nondestructive testing) technologies before use [101].

Magnetic flux leakage (MFL) testing is an electromagnetic nondestructive testing (NDT) method with high efficiency and reliability. It has the ability to detect various types of defects such as cracks, corrosion, pitting, and cavity, and it is able to detect both surface and subsurface defects. Therefore, it has been widely used to ensure the integrity and safety of structures in the petrochemical, energy, manufacturing, and transportation industries.

1. The principle of MFL testing is based on the interaction between magnetic field and defects. The MFL testing device usually consists of a magnetizing unit, a sensing unit, a signal conditioning unit, an analog-to-digital converter (ADC), and a computer with signal displaying and analyzing software. So, magnetizing coils are able to magnetize the ferromagnetic specimen into saturation or near saturation. Due to the abrupt change in magnetic reluctance at the defects, the magnetic flux leaks into the nearby air. The perturbation of the magnetic field can be recorded by an array of magnetic field sensors and used to evaluate and quantify defects.

In order to improve the inspection sensitivity, we demonstrate how to make an optimal choice of each device: magnetizing, sensing and signal processing, [xxx].

In this context, as a first stage, we study the effect of the geometrical and the electrical factors affecting the magnetizing system composed of Helmholtz coils such as the distance between the two coils, there average diameter and the DC exciting current intensity. In fact, this study is very important in order to create a uniform axial magnetic field in which the sensors will be placed.

After that, we make in evidence the factors affecting the magnetic field leakage signal shape and amplitude such as the Lift-off, the magnetization strength and defect size.

2.2. Description of the studied device

Drill pipes are made of high alloy materials and have a high hardness after heat treatment; thus, the drill pipes are hard to magnetize. Here, a Helmholtz coil magnetization method is largely used to produce a high and uniform magnetic field. In this paper, the inspection for the most widely used 5 in. drill pipes (material grade: X80; thickness: 9.19 mm; body diameter: 127.0 mm; pipe end diameter: 184.2 mm) is analyzed and conducted. The Helmholtz coil magnetizer are as follows: the internal diameter of the coil is 284.0 mm, the external diameter of the coil is 375.2 mm, the thickness of the coil is 100 mm, the distance between the two coils is 100 mm, and each coil has 6000 ampere-turn, respectively. The geometrical configuration of the studied system and the B-H curve X80 grade inspected pipe are given on Figure 15.

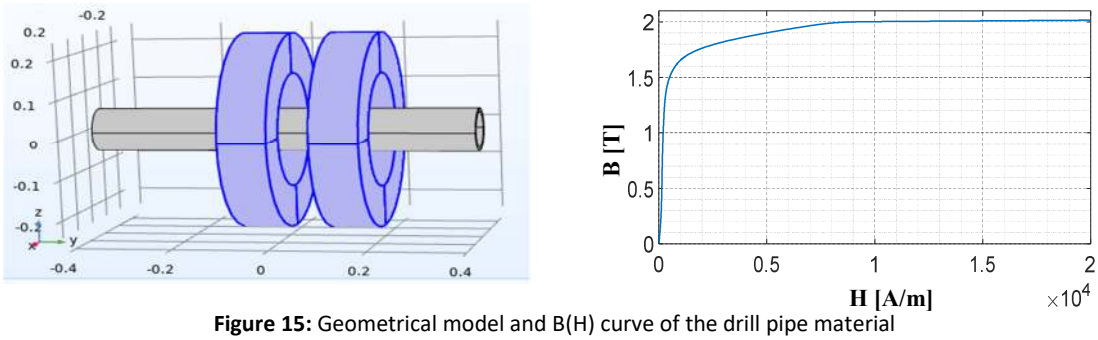

Figure 15: Geometrical model and B(H) curve of the drill pipe material

2.3. Simulation and analysis of the distribution of the magnetic field

After implementing the three-dimensional model under Comsol Multiphysics, we proceeded to the analysis of the distribution of the magnetic field in the active parts of the magnetization system and the tested pipe.

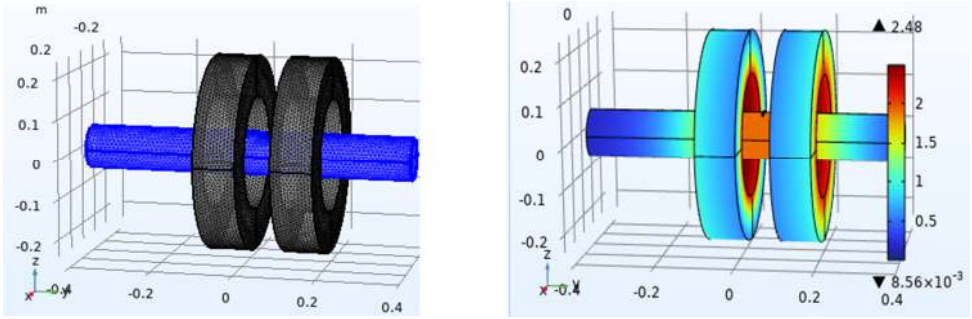

Figure 16: 3D mesh and distribution of the magnetic induction

On the other hand, the components of the magnetic field intensity along the three axes are shown in Figures 16.

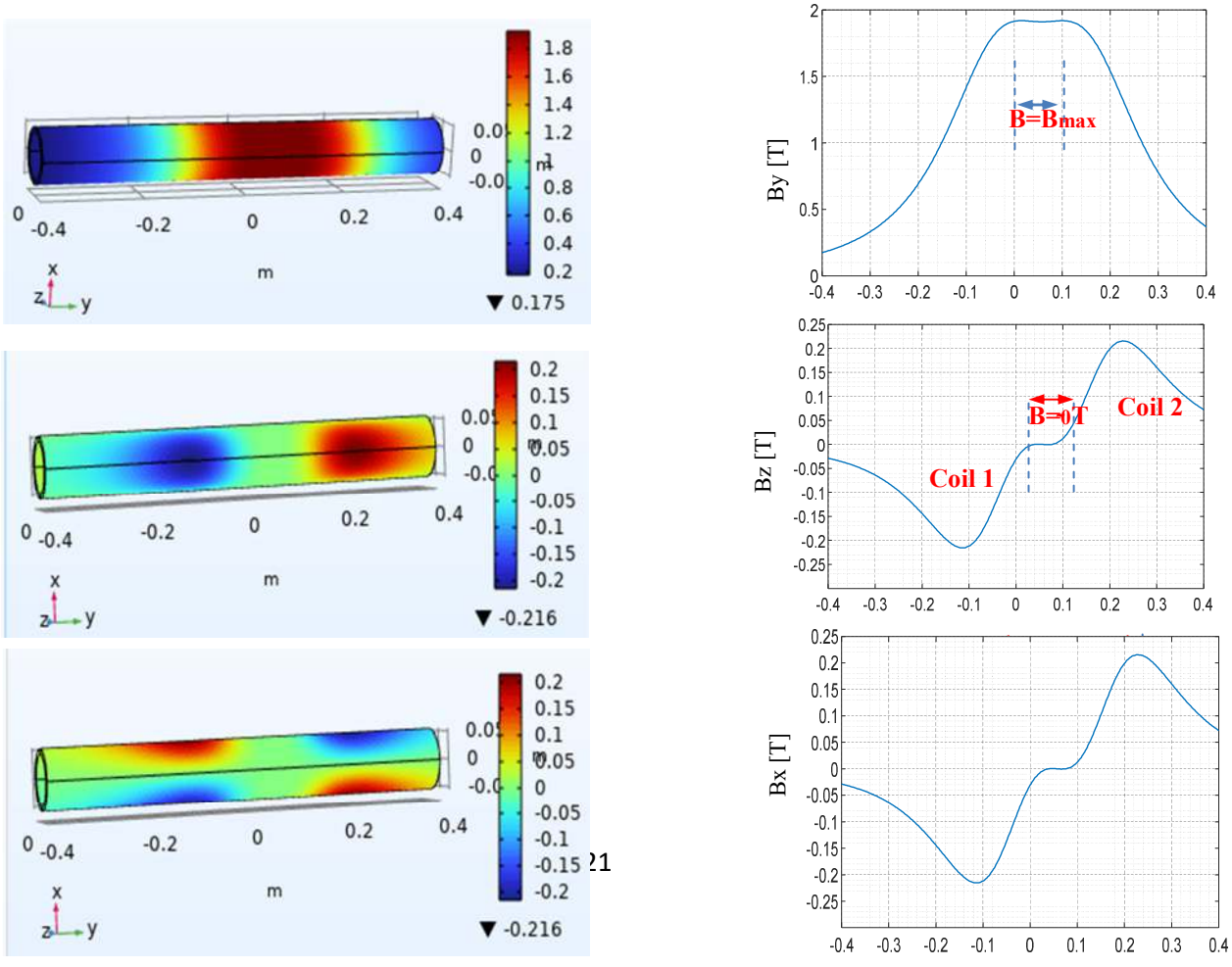

Y [m]

From the results shown in Figure 17, we can see clearly that the magnetic field is uniform in the zone **UFZ** (uniform field zon) located between the excitation coils and the drill pipe is magnetically saturated along the Oy axis (B=Bs). On the other hand, the magnetic field is very weak along Ox and Oz (B=0T). Indeed, this electromagnetic configuration leads to better detection of transverse defects such as cracks and pits. However, several factors influence the amplitude and shape of the magnetic field produced by the excitation coils; this will be the subject of the study in the next section.

Figure 17: Component of the magnetic induction following the Y axis.

2.4. Factors affecting the UFZ

In MFL inspection devices, the magnetic material to be inspected must be magnetized to saturation by referring to its B(H) curve shown in Figure 16 in order to be able to detect even small defects with high accuracy. On the other hand, obtaining a uniform field area allows the MFL field sensors to be placed in this area because a field variation necessarily indicates the presence of a defect. Indeed, we will study the main parameters influencing the shape and amplitude of the magnetic field such as the excitation current J, the inner radius R of the excitation coils as well as the distance D between them.

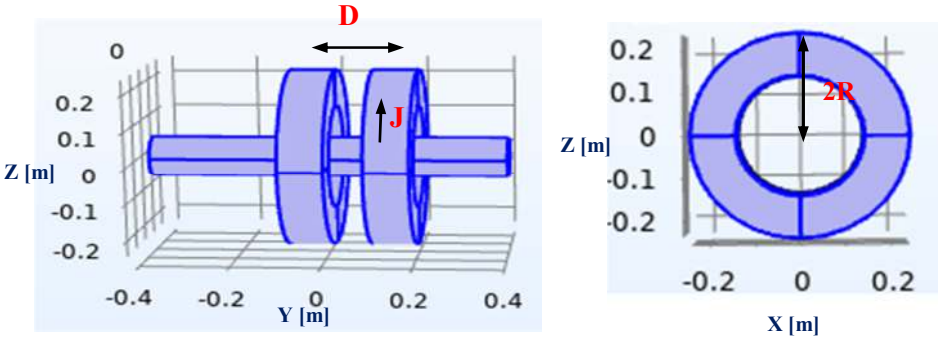

Figure 18: Geometrical configuration of the studied device

To do this, we vary each parameter while keeping the others fixed. Indeed, the simulation results are given in Figure. 19

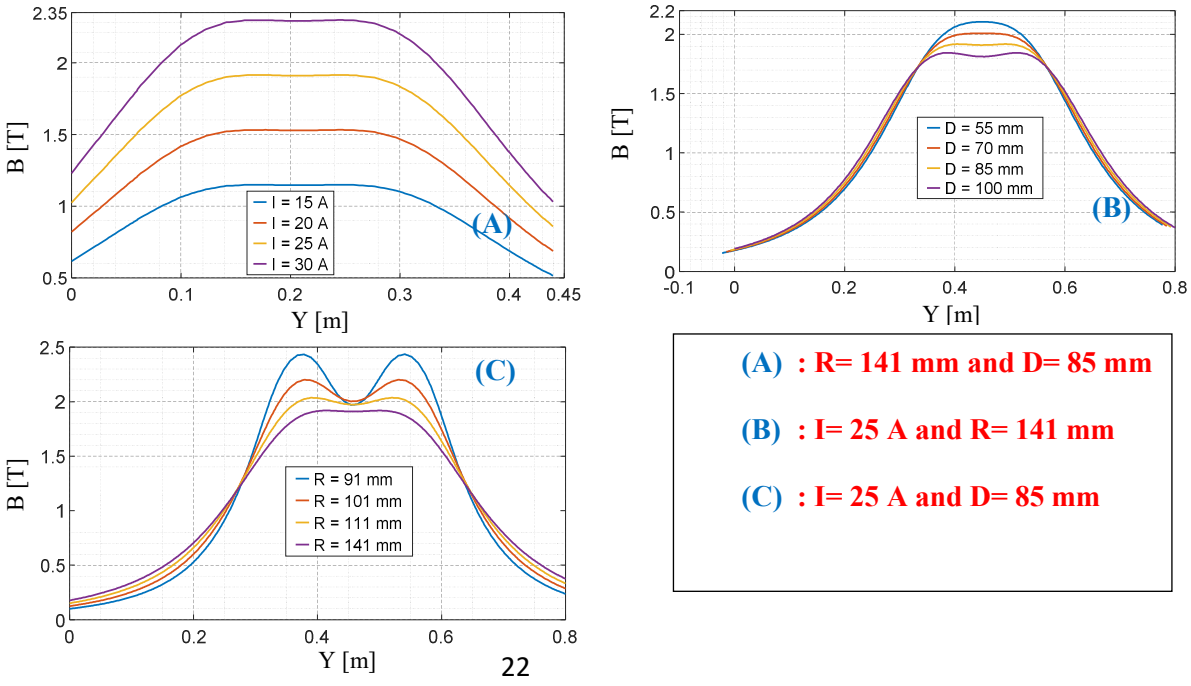

Figure 19: Norm of magnetic induction according to magnetization direction

By analyzing the results shown in the previous figures, we can see that:
- The amplitude of the excitation current only affects the amplitude of the magnetic induction in the steel pipe. When the current intensity increases from 15A to 30A the magnetic induction increases from 1.1T to 2.2T.
- Furthermore, the distance D and the radius R influence both the shape and amplitude of the uniform field zone. For example, the length of the UFZ increases from x1mm to x2mm when R increases from y1mm to y2mm, whereas the UFZ decreases in amplitude and increases from B=1T to B=2T. On the other hand, when D increases from D2 to D2, the length of the UFZ varies from L1 to L2 and the amplitude of B1. For this reason, a judicious choice must be made on these parameters to obtain the best characteristics. It should be noted that the dependence between these parameters can be interpreted by Ampere's law.

2.5. Detection of transverse defects in drilling pipes

To reach the black gold, drilling pipes have to penetrate deep into the earth. For medium-deep drilling of around 2000 m in depth, approximately 222 pipes of 9 m each are required. A new pipe has to be screwed on every 9 m. The material has to withstand a lot and be durable. Faultless material that meets international standards is thus essential. For this purpose one of the equipment that used to check the condition of pipes in the drilling industry is the EMI system which is actually the most accurate method to detect possible defects. Electromagnetic inspection (EMI), as a non-destructive testing method, can detect the presence of transverse defects and pits by inducing a magnetic field inside metal objects and collecting the resulting responses by a number of sensors, which they are placed around the body. Various magnetic field detection sensors such as pick-up coils, Hall sensors, magneto-diodes, fluxgates, anisotropic magneto-resistance (AMR) and Giant-magneto-resistive (GMR) sensors are commonly used in MFL technique [102]. Table 1 compares the performance of various sensors used.

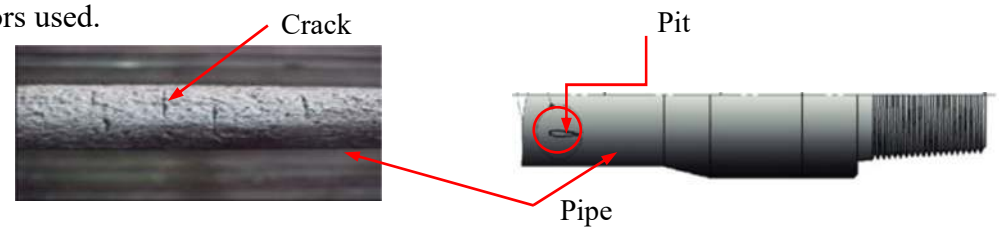

Figure 20: Norm of magnetic induction according to magnetization direction.

The most magnetic sensors used in the electromagnetic inspection (EMI) of drilling pipes are Pick-up coils and Hall sensor. Pick-up coil consist of some turns of copper wire wrapped around a core. They measure the change in magnetic field due to the presence of defects in the object. They have the advantages of being cheap, high flexibility in sensor configuration and no saturation even at quite large excitation levels. However, they are less sensitive. In other hand, Hall sensor is the most commonly used flux leakage sensors. It works on the principle of Hall effect and measures the normal component of the magnetic field. A typical Hall device consists of indium arsenide, indium antimony, gallium arsenide or silicon. It has the advantages of high linearity, small size, inexpensive, room temperature operation and fabrication of sensor arrays. However, they suffer from limited sensitivity and large offset. Recently, micro-Hall sensors are also used in MFL

NDE applications due to their high sensitivity and wide linear response [103].
In the following study, we calculate the MFL signal in the sector zone as shown in the following figure.

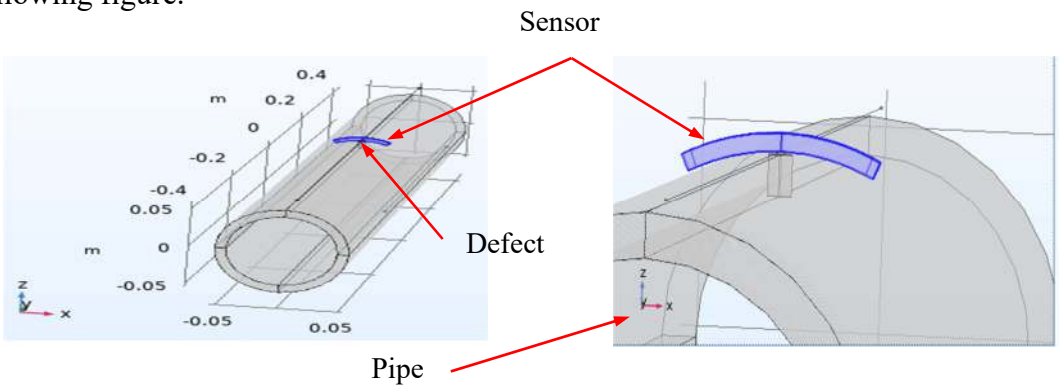

Figure 21: The inspected pipe, hole defect and magnetic sensor.

2.5.1. Effect of the exciting current intensity on MFL signal

In this section we proceed to study the effect of the defect size (Hole radius) on the MFL signal for the exciting coils current intensity of 20A and 25A. In fact, the MFL signal components according to the scanning positions are depicted in Figure 22.

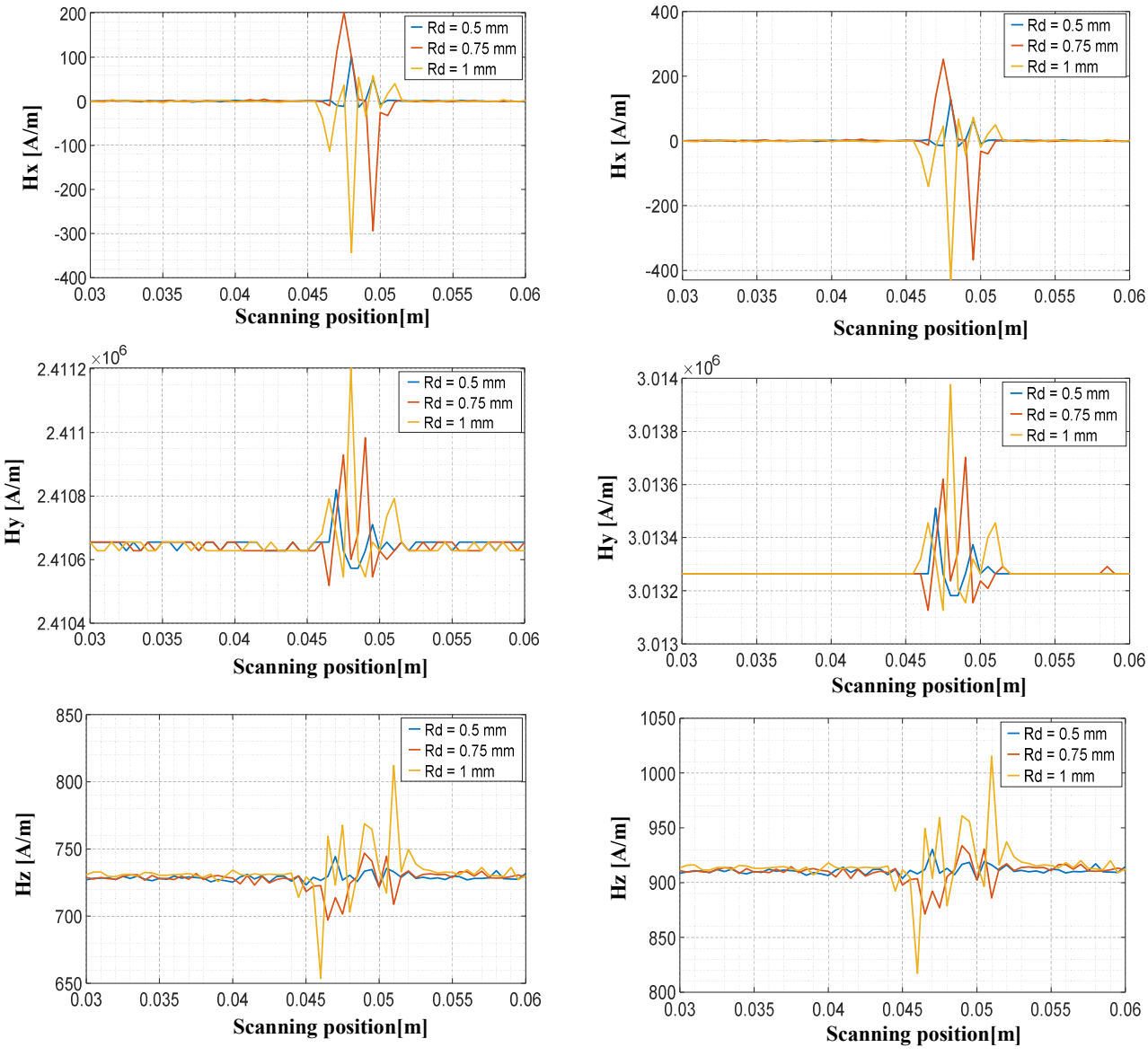

Figure 22: Components of the magnetic field (Hx, Hy and Hz) according to the defect radius Rd. (J=20A at the left and J= 25A at the right).

By looking to the previous results we can see clearly that :

- As well as the defect radius **R** increase the amplitude of the magnetic field leakage increase. However, other geometrical parameters can influence the signal amplitude such as the angle between the defect and magnetization field as explained by some researchers, [xx].
- An increasing in the exciting current intensity **I** of 5A induces a significant increase on the MFL components Hx, Hy and Hz amplitude. In fact, this can be explained by the fact that the magnetic induction in the tested pipe is about 1.5 T for the 20A and 1.9 T for 25A and the corresponding leakage field became greater. However, MFL signal does not always increase with the magnetization strength. Many researchers have demonstrated that the MFL signal initially increases with the magnetization current and start to decrease after a certain point because a strong magnetization suppresses the leakage of the magnetic field from defects, [xxx]. In addition, the offset value of each component changes according to the exciting current intensity (the greater value is obtained according to the magnetization direction Y).

2.5.2. Effect of the Lift-off on MFL signal

In this section we study the effect of Lift-off (distance between sensors and the pipes surface) on the components of the MFL signal. In fact, the MFL signal components according to the scanning positions for Rd=1mm and I= 25A are depicted in Figure 23.

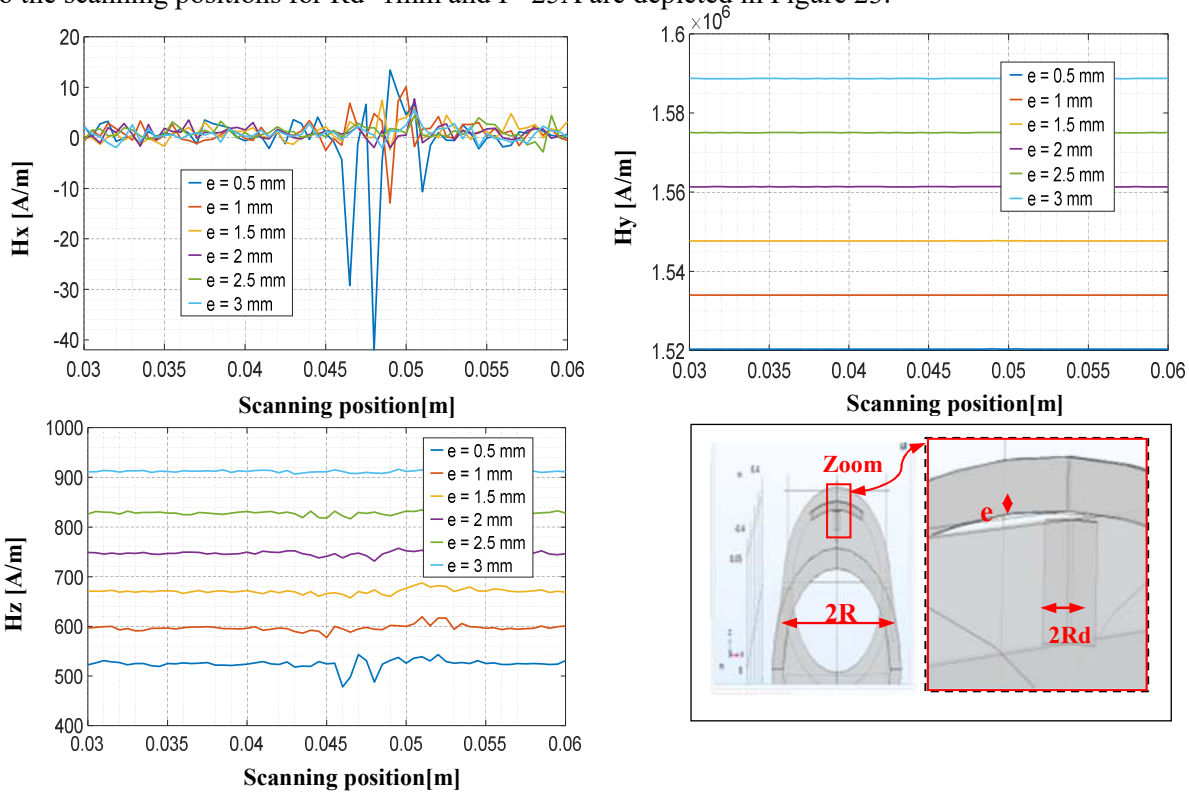

Figure 23: Components of the magnetic field according to Lift-off for J= 25 A, R = 85 mm and Rd= 1mm.

From these results, we can notice that the small Lift-off provide a higher values of the MfL and small Offset values. But, near-zero lift-off detection will evidently cause severe wear and even damage to the probe. For this reason, an optimal lift-off distance must be chosen. In this context, several works presented some solution such as magnetic shielding device and magnetic focusing effect, [104].

In addition, the change in liftoff during scanning significantly influences the testing signal. Thus, many researchers have attempted to reduce the liftoff effect such as filtering method and compensation, [xx].

The second remark is the presence of the permanent MFL signal. For this reason the inductive sensors with a specific configuration is more adapted because it allow us to eliminate the permanent magnetic field and measure MFL of high amplitude.

2.6. Conclusion

In this chapter we have implemented a 3D magnetic field leakage system of inspection of drilling pipe in Comsol-multiphysics software. In first stage, we have studied the effect of some geometrical and electrical parameters of the exciting coils on of the magnetization process such as the amplitude and the shape of the magnetic field in the uniform field zone (UFZ). In the second stage, we have demonstrated by numerical simulation the factor affecting the MFL signals.

In fact, through the obtained results we can conclude that:

- The amplitude of the excitation current only affects the amplitude of the magnetic induction in the steel pipe. When the current intensity increases from 15A to 30A the magnetic induction increases from 1.1T to 2.2T.

- Furthermore, the distance D and the radius R influence both the shape and amplitude of the uniform field zone. For example, the length of the UFZ increases from x1mm to x2mm when R increases from y1mm to y2mm, whereas the UFZ decreases in amplitude and increases from B=1T to B=2T. On the other hand, when D increases from D2 to D2, the length of the UFZ varies from L1 to L2 and the amplitude of B1. For this reason, a judicious choice must be made on these parameters to obtain the best characteristics. It should be noted that the dependence between these parameters can be interpreted by Ampere's law.

- As well as the defect radius **R** increase the amplitude of the magnetic field leakage increase. However, other geometrical parameters can influence the signal amplitude such as the angle between the defect and magnetization field as explained by some researchers, [xx].
- An increasing in the exciting current intensity **I** of 5A induces a significant increase on the MFL components Hx, Hy and Hz amplitude. In fact, this can be explained by the fact that the magnetic induction in the tested pipe is about 1.5 T for the 20A and 1.9 T for 25A and the corresponding leakage field became greater. However, MFL signal does not always increase with the magnetization strength. Many researchers have demonstrated that the MFL signal initially increases with the magnetization current and start to decrease after a certain point because a strong magnetization suppresses the leakage of the magnetic field from defects, [xxx]. In addition, the offset value of each component changes according to the exciting current intensity (the greater value is obtained according to the magnetization direction Y).

- The small Lift-off provide a higher values of the MfL and small Offset values. But, near-zero lift-off detection will evidently cause severe wear and even damage to the probe. For this reason, an optimal lift-off distance must be chosen. In this context, several works presented some solution such as magnetic shielding device and magnetic focusing effect, [105]. In addition, the change in liftoff during scanning significantly influences the testing signal. Thus, many researchers have attempted to reduce the liftoff effect such as filtering method and compensation, [xx].

- Due to the presence of the permanent MFL signal. For this reason the inductive sensors with a specific configuration is more adapted because it allow us to eliminate the permanent magnetic field and measure MFL of high amplitude.

3. Chapter III

3.1. Introduction:

EMI inspection method is an NDT application applied to tubular products such as tubing and drill pipe. It involves full length scanning of tubes using a coil to induce longitudinal field with a buggy type unit to detect transverse flaws in the material, which includes flaws such as fatigue cracks, corrosion, pits, cuts, gouges, and other damage that exceed the specified acceptance limits. If flaws are present, the induced field will create flux leakage at the point of flaw. The leakage is detected by hall effect probes on the buggy which transmits a signal to a computer console. The signal is then evaluated by a trained inspector.

Our work in this chapter consists of conducting practical tests with an MFL inspection device available from the national drilling company ENAFOR. In the first step, we present the inspection device, which consists of a magnetization system, the leakage field sensors, and the motor responsible for moving the assembly along the drill pipe. We then study the effect of speed and lift-off on the shape and amplitude of the leakage field measured by the eight magnetic sensors.

3.2. Presentation of the electromagnetic inspection device

The VEDAQ 2000-C™ is a portable, computerized, multi-function EMI system for inspecting drill pipe and tubing. Transverse flaw detection and TRUEWALL™ solid state (Hall effect) wall monitoring functions are standard on the VEDAQ 2000-C™. It's lightweight, compact and extremely portable design allows the VEDAQ 2000-C™ to be operated at the rig site or in a pipe yard. Commands (i.e. gain, coil, buggy adjustments) are controlled on the computer. The inspection results are displayed digitally in the software with individual channel colors for easy interpretation. The VEDAQ 2000-C™ is designed to meet most industry requirements set forth by API, DS-1, etc.

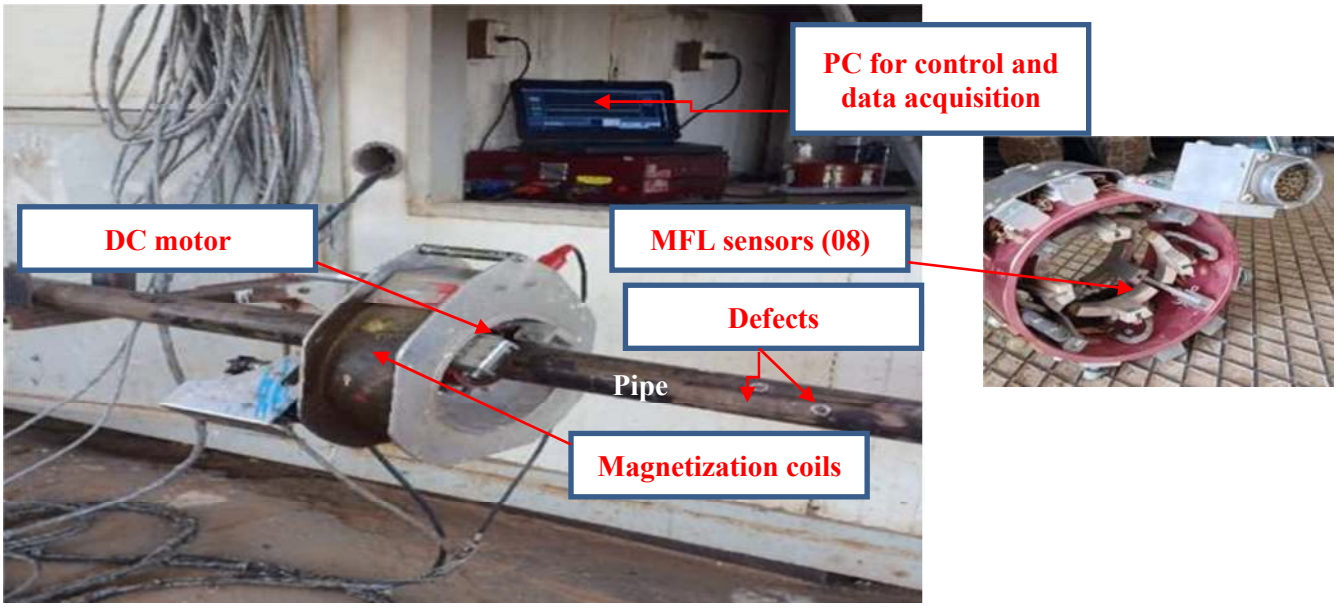

Figure 24: EMI system components.

The main characteristics of the each component are given on the figure 25.

Capacity:	2 3/8" to 6 5/8" O.D. drill pipe and tubing
Functions:	1) Transverse (TV) flaw detection (cracks and pits) 2) TRUEWALL™ magnetic wall thickness monitoring
Production Rate:	Up to 150 Ft. per minute, all functions
Inspection Criteria:	The VEDAQ 2000-C™ is designed to meet most stringent industry requirements set forth by API, DS-1, etc.
Major Components:	1) Electronics console with 2-function circuitry 2) Detector shoe (buggy) heads (sizes optional) 3) High-speed buggy drive with variable speed DC motors 4) Powerful DC magnetizing coils 5) Air jack set (standard or Hi-Low models available) 6) Calibration standards (optional)
Data Acquisition:	PC-based data acquisition system with ruggedized laptop computer (all functions performed on computer with multi-color data display).

Buggy Head 2 3/8" - 6 5/8"

Figure 25: Characteristics of the EMI device.

3.3. Mode of operation

The system is calibrated on a standard at the beginning of the job. First the pipe transported by the conveyor is placed on the racks (**step A**). The magnetizing coil is placed over the end of the pipe (**step B**). The buggy drive and head are placed on top of the pipe and the mag coil is placed on the buggy drive (**step C**). The air jacks lift the pipe so the coil & buggy will clear the pipe racks (**step D**). The electronics operator then powers the buggy down the pipe and starts the computer while observing the data on the software (**step E**). When the buggy reaches the other end of the pipe, the jacks lower the pipe to the racks (**step F**). Finally, the buggy and coil are removed and placed on the next pipe. The process is then repeated in the opposite direction.

The previous steps are shown on the figure 26.

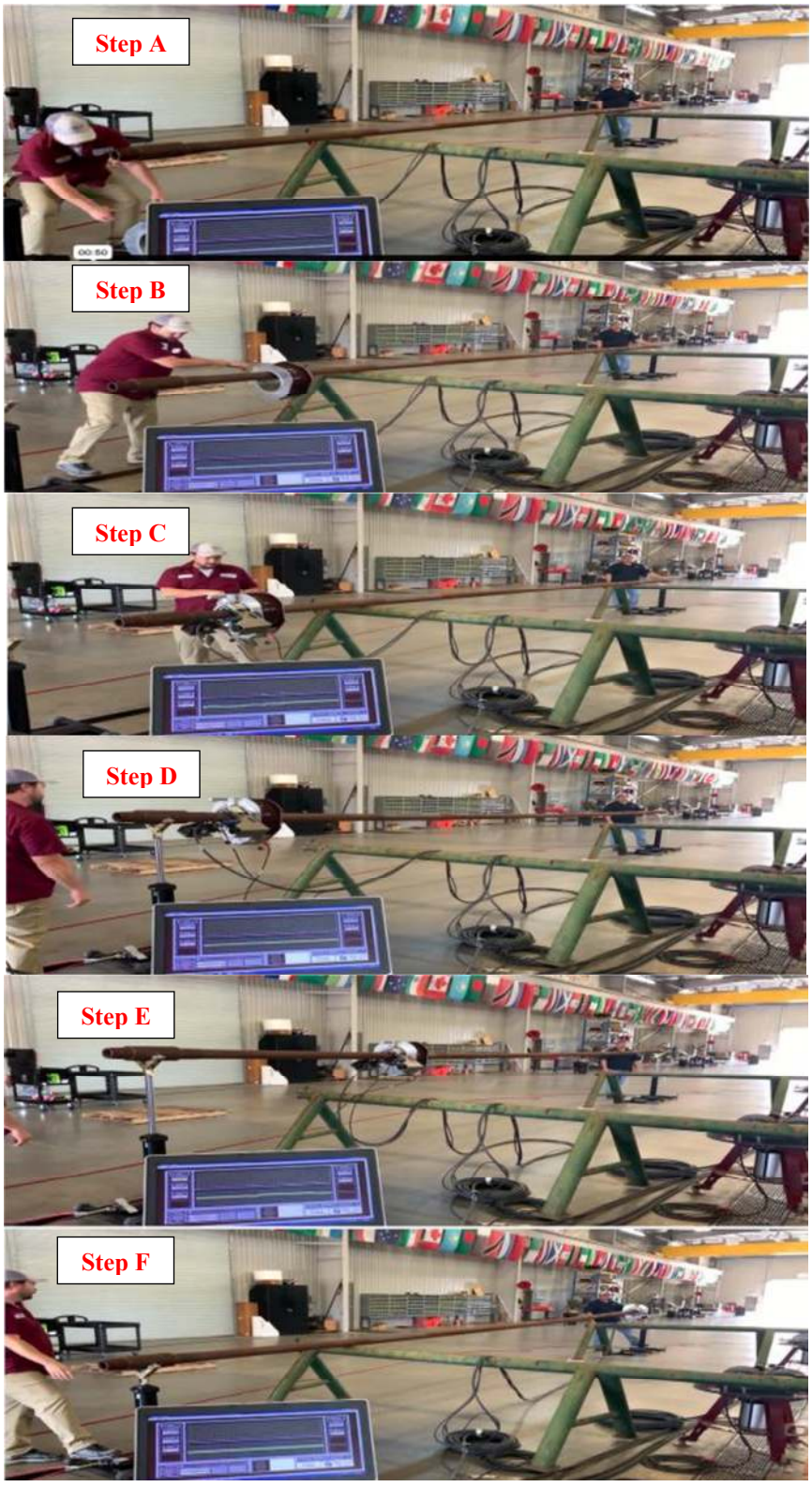

Figure 26: Mode of operation steps

3.4. Effect of the scanning speed

In MFL (Magnetic Flux Leakage) inspection, scanning speed significantly impacts the strength and interpretation of the leakage signal, [xx]. In this section our objective is to study the effect of the scanning speed on the shape and the amplitude of the MFL signal. For this reason, we realize three scanning of different speed: 30/, 60/ and 100/. So, the obtained results

are given on the following figure.

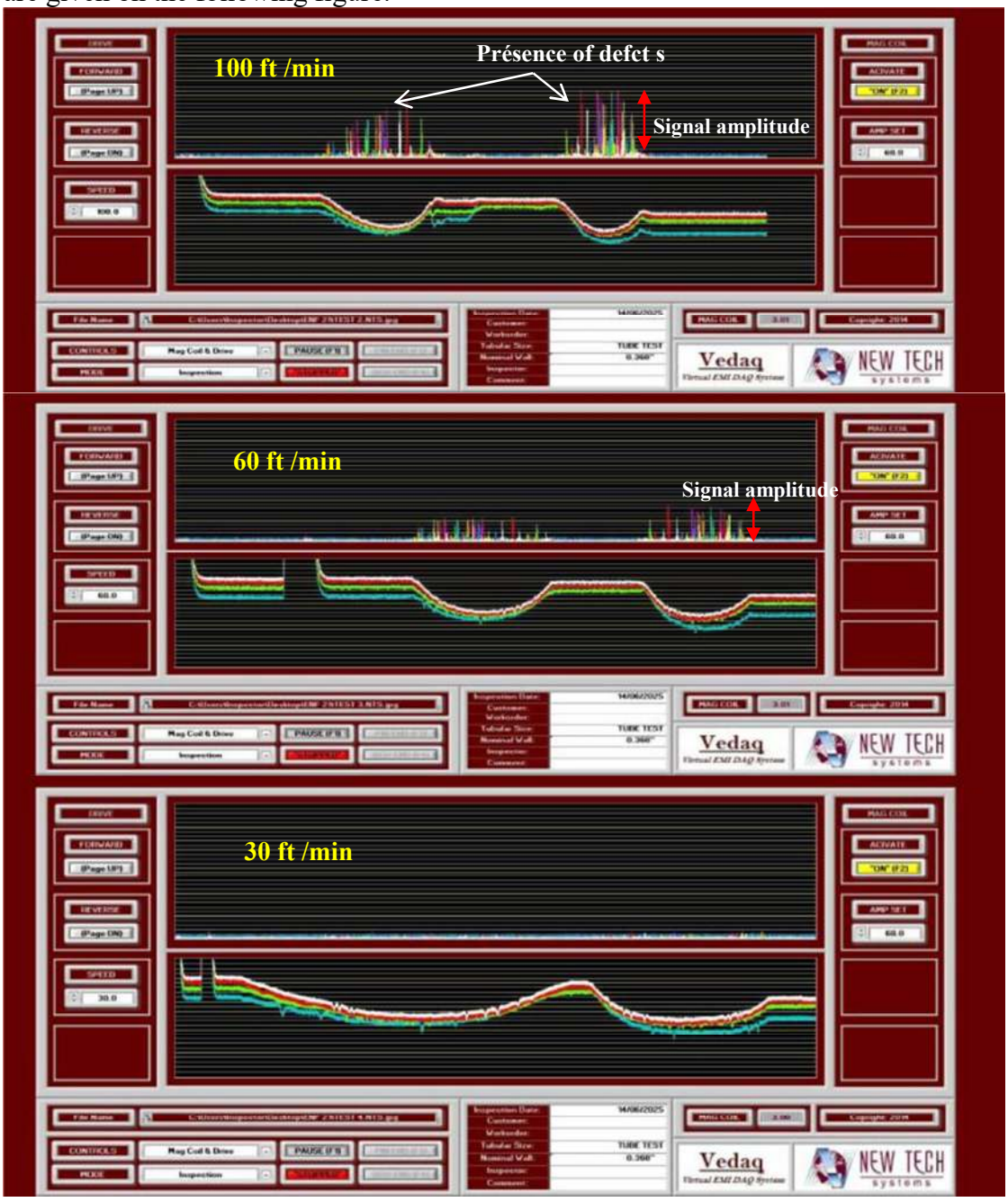

Figure 27: MFL signals along the drill pipe for different scanning speed.

The obtained results are in concordance with those published in literature because near-surface defect signals may increase at higher speeds due to flux concentration near the surface, but this can lead to signal clipping if the sensor range isn't sufficient. Therefore, optimal scanning speed is crucial for accurate defect detection and characterization.

3.5. Effect of Lift-off

The MFL signal is dependent on the liftoff distance between the probe and the specimen. The MFL signal reduces as the increase in liftoff distance [xx].The change in liftoff during scanning significantly influences the testing signal. Thus, many researchers have attempted to reduce the liftoff effect. Jia used a filtering method to suppress lift-off interference [106]; Wu proposed a liftoff tolerant sensor by inserting ferrite into the sensing coil [107]; Peng

introduced an exponential function compensation for lift-off correction [108]; Wang linearized the liftoff effect by applying Fourier transformation.

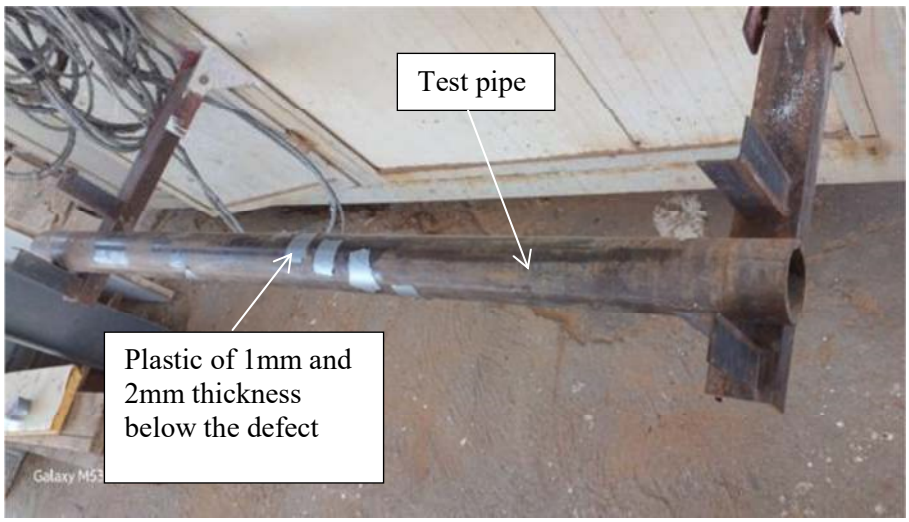

Figure 28: Creation of an artificial Lift-off with a thin plastic.

This experience is done for a scanning velocity of 100ft/min while the artificial Lift-off is about 0mm, 1mm and 2mm. the obtained results are given on the following figure.

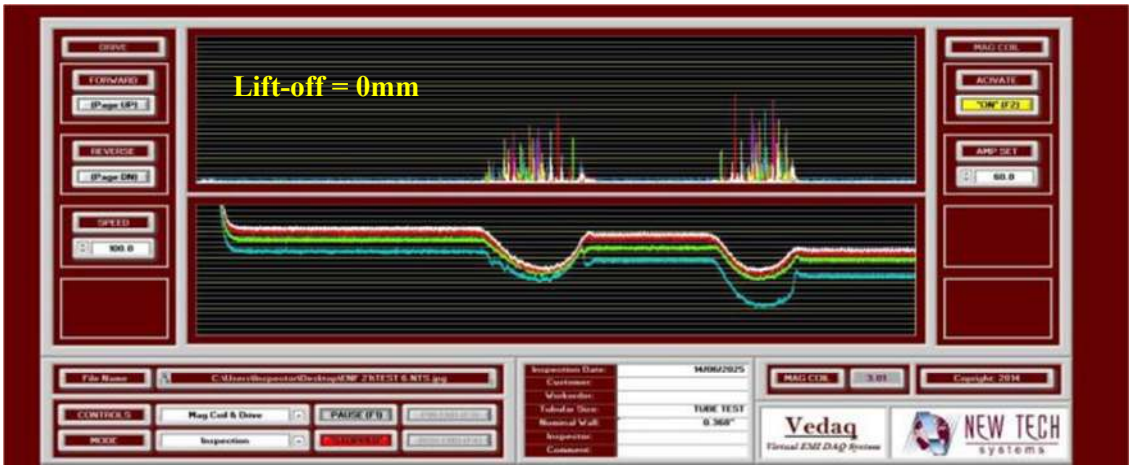

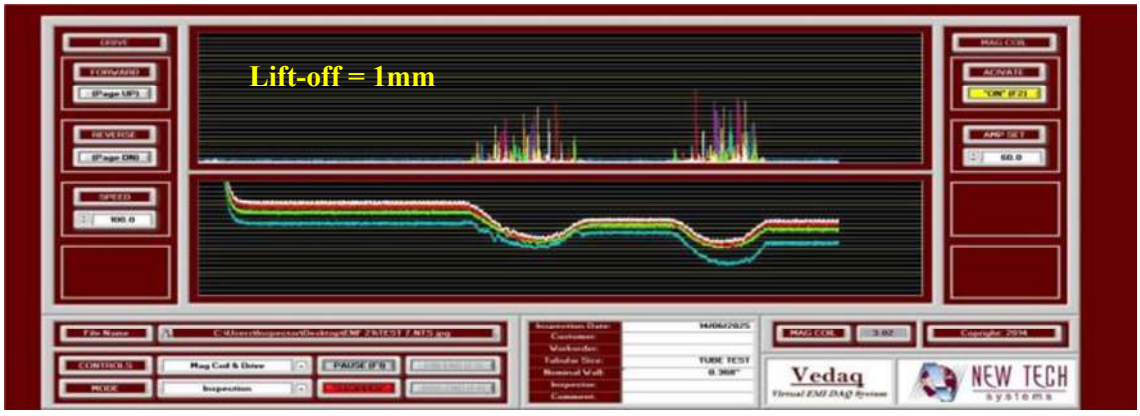

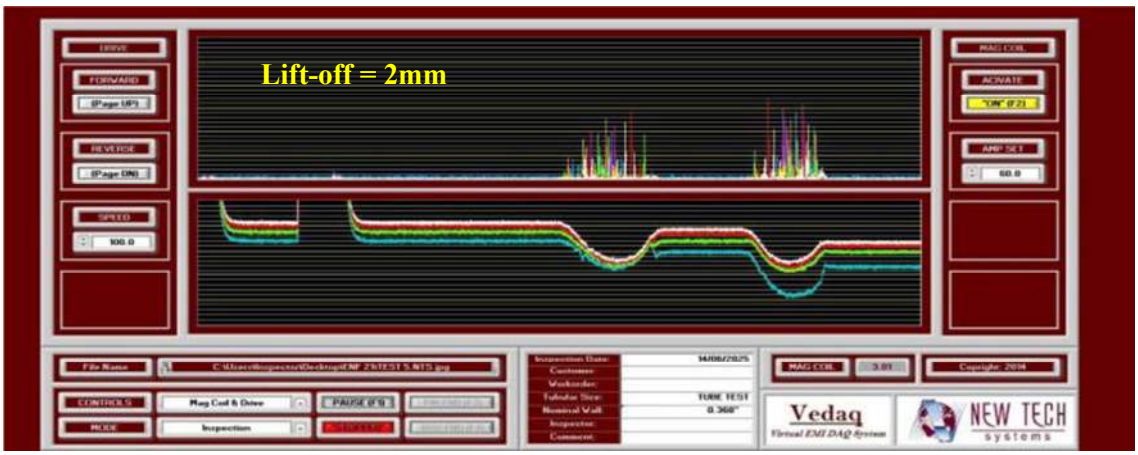

Figure 29: MFL signal according to scanning position for different Lif-off.

From the previous results we can confirm that this device compensates perfectly Lift-off variations, which results in the stability of the MFL signal. However, drill pipes cleaning must be done before inspection because the effect of magnetic particles distorts significantly the measurements.

3.6. Conclusion

In this chapter, we presented the steps to follow in order to achieve experimental tests of drill pipe inspection using a VEDAQ-2000 EMI device available at ENAFOR. Also, we have presented the essential elements of an EMI test unit such as the Helmholtz coil magnetization device, the leakage field sensors, and the interface data acquisition. After that, we have studied the influence of several parameters, such as scan speed and the distance between the sensors and the drill pipe surface (Lift-off) on detection sensitivity. The obtained results show a good concordance with those published in the literature.

General conclusion

Nondestructive testing based on magnetic flux leakage (MFL) has recently been widely used in various fields of industry, where the problem of the inspection of products and elements from ferromagnetic materials arises. Intrinsic examples are magnetic inline nondestructive testing and nondestructive testing of steel wire ropes, steel storage tanks, and drill pipes. The instruments for performing this method are manufactured by various companies, including Rosen, Silverwing, NDT Technologies, Intron Plus, and others. The principal advantages of this method are that it allows the detection of uniformity flaws of a material both on surface and along the thickness of the product (a pipe and plate wall or rope section) in the presence of a sufficient gap between the sensor and the product (several mm); this provides high productivity of such inspection, [ref Data Processing and Representation in the MFL].

Through this study the following conclusions were drawn:

- The Helmholtz concentrating field system must be chosen as function of drill pipe diameter and B(H) curve. In addition, the amplitude and the uniformity of the uniform field zone depend on coils diameter, distance between each ones and the exciting current intensity.
- Lift-off variation affect MFL signal by reducing its amplitude. But, this phenomenon can be surmounted by using some solutions such as using ferrite core sensors.
- The operator must choose an optimal scanning velocity in order to reduce the effect of eddy current and noise signals. So, in modern EMI devices these specifications are available on manual guide.

We notice that this study can be extended as follow:

- Developing an optimization algorithm for designing magnetization system (coils) based on the geometric and magnetic parameters of the tubes.
- Creating the experimental setup for defect detection and thickness monitoring (this detail will be discussed in September).
- While using an appropriate algorithm, we can classify the defect level from MFL signal amplitude.

REFERENCES

[1] Baldev Raj. T. Jayakumar, M. Thavasimuthu. Practical Non-Destructive Testing. Third Edition, Narosa, New Delhi, 2012

[2] D L Atherton, "Magnetic inspection is key to ensuring safe pipelines," Oil Gas J, 87, no.32, 1989, pp. 52-61.

[3] N. Kasai, K. Sekine and H. Maruyama, "Non-destructive evaluation method for far-side corrosion type flaws in oil storage tank bottom floors using the magnetic flux leakage technique", Journal of the Japan Petroleum Institute, vol. 46 (2), 2003, pp. 126-132.

[4] Satish S Udpa and Patrick O Moore, Nondestructive Testing Handbook, Vol. 5 Electromagnetic Testing. ASNT 3rd Edition, 2004, p. 230.

[5] R.E Beissner, G.A. Matzkanin and C.M. Teiler. "NUE Applications of magnetic leakage field methods, a state-of-the-art survey", NTIAC-80-1. January 1980.

[6] G. Dobmann, "Magnetic Leakage Flux Techniques in NDT A State-of-the-Art Survey of the Capabilities for Defect Detection and Sizing", Electromagnetic Methods of Nondestructive Testing. Edited by William Lord. Gordon and Breach, 1985, pp. 71-95.

[7] D.C. Jiles, "Review of magnetic methods for nondestructive evaluation (Part 2)", NDT International, vol. 23, no. 2. April 1990, pp. 83-92.

[8] Jack Blitz, "Electrical and Magnetic Methods of Nondestructive Testing". Adam Hilger publication, 1997.

[9] Masatoshi Kuroda, Shinsuke. Yamanaka, Koji Yamada, Yoshihiro Ische, "Evaluation of residual stresses and plastic deformations for iron-based materials by leakage magnetic flux sensors", Journal of Alloys and Compounds 314, 2001, pp. 232-239.

[10] N.N. Zatsepin and V.E. Shcherbinin, "Calculation of the Magnetostatic Field of Surface Defects. 1. Field Topography of Defect Models", Defektoskopiya, no. 5, 1966, pp. 50-59.

[11] V.E. Shcherbinin and A.I. Pashagin, "Fields of defects on the inner and outer surfaces of a tube during. circular magnetization", Sov J NDT 8. 1972, p. 134.

[12] V.E. Shcherbinin and A.I. Pashagin, "Influence of the extension of a defect on the magnitude of its magnetic field", Sov J NDT 8, 1972. p. 441.

[13] I.A. Novikova and N.V. Miroshin, "Investigation of the Fields of Artifical open flaws in a uniform constant magnetic field", Defectoskopia, 4, August 1973, pp. 95-101.

[14] F. Forster, "Nondestructive inspection by the method of magnetic leakage fields", Defektoskopiya 11, 1982, pp. 3-25

[15] Y. Zhang, K. Sekine and S. Watanable, "Magnetic leakage field due to sub-surface defects in ferromagnetic specimens", NDT & E International, vol. 28, no.2, 1995, pp. 67-71.

[16] S.M. Dutta, F.H. Ghorbel and R.K.Stanley. "Dipole modeling of magnetic flux leakage", IEEE Transactions on Magnetics, vol. 45, no. 4, April 2009, pp. 1959-1965.

[17] B. Bruder, "Magnetic Leakage Fields Calculated by the Method of Finite Differences", NDT International, vol. 18, no. 6, December 1985, pp. 353-358.
[18] J.H. IIwang and W. Lord, "Finite element modeling of magnetic field-defect interactions", J. Test & Eval, 1975. p. 21.

[19] W. Lord and J.H. Hang. "Defect characterization from magnetic leakage fields", British J NDT 19, Jan. 1977, pp. 14-18.

[20] W. Lord, J.M. Bridges, W. Yen and R. Palanisamy, "Residual and active leakage fields around defects in ferromagnetic materials", Mater Fval 36, 1978, p. 47.

[21] Nathan Ida, William Lord, "3-D Finite Element Predictions of Magnetostatic Leakage Fields", IEEE Transactions on Magnetics, vol. Mag 19, no. 5, September 1983, pp. 2260-2265.

[22] D.L Atherton, and M.G. Daly, "Finite element calculations of magnetic flux leakage detector signals", NDT International 20, 1987, pp. 235-238.

[23] Gerard Meunier, The finite element method for electromagnetic modeling, Wiley, 2008.

[24] W. Sharatchandra Singh, B.P.C. Rao, S. Vaidyanathan, T. Jayakumar and Baldev Raj, 'Detection of Leakage Magnetic Flux from Near-side and Far-side Defects in Carbon Steel Plates using Giant-magnetoresistive Sensor', Measurement Science and Technology 19 (2008) 015702 (8pp).

[25] M.N. Baibich, J.M. Broto, A.Fert, F.Petroff, P.Eitenne, G.Creuzet, A.Friederich, and J.Chazelas, "Giant Magnetoresistance of (001) Fe/(001) Cr Magnetic Superlattices", Phys. Rev. Lett., vol. 61, No.21, 1988, pp. 2472-2475.

[26] W. Sharatchandra Singh, K. Krishna Nand, B. P. C. Rao, T. Jayakumar and Baldev Raj, "Magnetic flux leakage NDE using giant magnetoresistive (GMR) sensors", Review of Progress in Quantitative NDE, AIP Press, 27B (2007), 857-864,
[27] Ch. Ravi Kumar, B.P.C. Rao, T.S. Abhilash, G. Rajaram, T. Jayakumar and Baldev Raj, Generic HEMT structure wafer Hall-magnetic sensors for magnetic flux leakage imaging for NDE of Magnetic Steels, Proc. of Int. Conf. on Materials for Advanced Technologies, Singapore, July 2007.

[28] W. Sharatchandra Singh, B.P.C. Rao, T. Jayakumar and Baldev Raj. "Simultaneous Measurement of Tangential and Normal Components of Leakage Magnetic Flux using Giant Magneto-resistive Sensors". Submitted to the IEEE transactions on magnetic, January, 2010.

[29] Jiseong Hwang, Jinyi Lee and Seokjin Kwon, "The application of a differential-type Hall sensors array to the nondestructive testing of express train wheels", NDT&E International 42, 2009, pp. 34-41.

[30] S O'Connor, L Clapham and P Wild, "Magnetic flux leakage inspection of tailor-welded blanks", Meas. Sci. Technol. 13, 2002, pp.157-162.

[31] Z Liu, Y Kang, X Wu and S Yang. "Study on local magnetization of magnetic flux leakage testing for storage tank floors", Insight, vol. 45, no. 5, May 2003, pp. 328-331.

[32] H. R. Weischedel and R. P. Ramsey. "Electromagnetic testing, a reliable method for the inspection of wire ropes in service', NDT International, June 1989, pp. 155-161.

[33] C. Jomdecha and A. Prateepasen. "Design of modified electromagnetic main-flux for steel wire rope inspection', NDT & E International, vol. 42, 2009, pp. 77-83.

[34] E. Kalwa and K. Piekarski, 'Design of inductive sensors for magnetic testing of steel ropes', NDT International, vol. 20, по. 6, December 1987, pp. 347-353.

[35] W. Sharatchandra Singh, B. P. C. Rao, C. K. Mukhopadhyay and T. Jayakumar, "GMR based magnetic flux leakage technique for condition monitoring of steel track rope".

[36] W. Sharatchandra Singh, Optimization of GMR Array Sensor based Magnetic Flux Leakage Techniques using Finite Element Modeling. Ph D Dissertation, HBNI, 2013

[37] KS Ryu, D L Atherton and L. Clapham, "Effect of pit geometry and bulk stress on near-and far-side calculated MFL signals", J. Phys.D: Appl. Phys. 35(2002) pp. 2693-2697.

[38] L. Clapham, V. Babbar and J. Byrne, "Detection of mechanical damage using the magnetic flux leakage techniqu 0 (www.physics.queensu.ca/-lynann/references/conference4.pdf)

[39] R. J. Davis and J. B. Nestleroth, "The Feasibility of Using the MFL Technique to Detect and Characterize Mechanical Damage In Pipelines," Review of Progress in Quantitative Nondestructive Evaluation, vol. 16. Plenum New York, 1997.

[40] S. Mandayam L. Udpa, S. S. Udpa and W. Lord. "Wavelet-based permeability compensation technique for characterizing magnetic flux. leakage images". NDT&E International,

[41] S. Mukhopadhyay, G.P. Srivastava, "Characterisation of metal loss. defects from magnetic flux leakage signals with discrete wavelet transform", NDT&E International 33, 2000, pp. 57-65.

[42] Muhammad Afzal, Satish Udpa, "Advanced signal processing of magnetic flux leakage data obtained from seamless gas pipeline", NDT&E International 35, 2002, pp. 449-457.

[43] A. A. Carvalho, J.M.A. Rebelloa, L.V.S. Sagrilob, C.S. Camerinic, I.V.J. Mirandad, "MFL signals and artificial. neural networks applied to detection and classification of pipe weld defects", NDT&E International 39, 2006, pp. 661-667.

[44] R. Christen and A. Bergamini, "Automatic flaw detection in NDE signals using a panel of neural networks", NDT&E International, vol. 39, Iss: 7, October 2006, pp. 547-553

[45] B.P.C. Rao, S. Thirunavukkarasu, K.
Krishna Nand. T. Jayakumar. P.Kalyanasundaram and Baldev Raj. "Enhancement of Magnetic Flux Leakage Images of Sub-surface Defects in Carbon Steel Using Eigen Value based Approach", Nondestructive Testing and Evaluation, vol. 35, 2007, pp. 35-42.

[46] K. Hwang. "3-D defect profile reconstruction from magnetic flux leakage signatures using wavelet basis function neural networks," Ph.D. dissertation, lowa State Univ., Ames, 2000.

[47] P. Ramuhalli, L. Udpa, and S.S. Udpa. "Electromagnetic NDC Signal Inversion by Function-Approximation Neural Networks", IEEE Trans. Magn.. 2002, vol. 38, по. 6, pp. 3633-3642.

[48] W. Han and P. Que, "An Improved Genetic Local Search Algorithm for Defect Reconstruction from MFL Signals". Russian Journal of Nondestructive Testing, vol. 41, no. 12, 2005, pp. 815-821.

[49] R. Baskaran, M. Pattabiraman, MP. Janawadkar, "Imaging defects in a three dimensional magnetically permeable medium using pseudoinverse technique". J Appl Phys, 2006:100:064909-11.

[50] R. Baskaran, M.P. Janawadkar, "Defect localization by orthogonally projected multiple signal classification approach for magnetic flux leakage fields". NDT&E International Vol. 41, 2008, pp. 416-419.

[51] Ali Sophian, Gui Yun Tian and Sofiane Zairi, "Pulsed magnetic flux leakage techniques for crack. detection and characterization", Sensors and Actuators A, Vol. 125, 2006. pp. 186-191.
52. Suresh, V.; Abudhair, A. Dipole Model to Predict the Rectangular Defect on Ferromagnetic Pipe. J. Magn. 2016, 21, 437–441. [CrossRef]
53. Katragadda, G.; Si, J.T.; Lord, W.; Sun, Y.S.; Udpa, S.; Udpa, L. A Comparative Study of 3D and Axisymmetric Magnetizer Assemblies Used in Magnetic Flux Leakage Inspection of Pipelines. IEEE Trans. Magn. 1996, 32, 1573–1576. [CrossRef]
54. Huang, S.; Li, L.; Yang, H.; Shi, K. Influence of Slot Defect Length on Magnetic Flux Leakage. J. Mater. Sci. Technol. 2004, 20, 231–232.
55. Sun, Y.; Kang, Y. The Feasibility of MFL Inspection for Omni-Directional Defects under a Unidirectional Magnetization. Int. J. Appl. Electromagn. Mech. 2010, 33, 919–925. [CrossRef] 56. Song, K.; Kang, Y.; Sun, Y.; Qiu, C.; Su, J. MFL Testing of Omni-Directional Cracks in Steel Strip Using Strong Longitudinal Magnetization. Int. J. Appl. Electromagn. Mech. 2010, 33, 1231–1236. [CrossRef]
57. Wu, J.; Sun, Y.; Kang, Y.; Yang, Y. Theoretical Analyses of MFL Signal Affected by Discontinuity Orientation and Sensor-Scanning Direction. IEEE Trans. Magn. 2015, 51, 1–7. [CrossRef]
58. Azizzadeh, T.; Safizadeh, M.S. Investigation of the Lift-off Effect on the Corrosion Detection Sensitivity of Three-Axis MFL Technique. J. Magn. 2018, 23, 152–159. [CrossRef]
59. Lunin, V.; Alexeevsky, D. Numerical Prediction of Signal for Magnetic Flux Leakage Benchmark Task. In Proceedings of the Review of Quantitative Nondestructive Evaluation, Green Bay, WI, USA, 27 July–1 August 2003; Volume 22, pp. 1830–1836.
60. Jia, Y.; Lu, Y.; Xiong, L.; Zhang, Y.; Wang, P.; Zhou, H. A Filtering Method for Suppressing the Lift-Off Interference in Magnetic Flux Leakage Detection of Rail Head Surface Defect. Appl. Sci. 2022, 12, 1740. [CrossRef]
61. Wu, J.; Fang, H.; Li, L.; Wang, J.; Huang, X.; Kang, Y.; Sun, Y.; Tang, C. A Lift-off-Tolerant Magnetic Flux Leakage Testing Method for Drill Pipes at Wellhead. Sensors 2017, 17, 201. [CrossRef]
62. Peng, L.; Huang, S.; Wang, S.; Zhao, W. A Simplified Lift-Off Correction for Three Components of the Magnetic Flux Leakage Signal for Defect Detection. IEEE Trans. Instrum. Meas. 2021, 70, 6005109. [CrossRef]
63. Wang, J.; Li, E.; Wu, J.; Xu, X. Linearization of the Lift-off Effect for Magnetic Flux Leakage Based on Fourier Transform. Meas. Sci. Technol. 2021, 32, 065012. [CrossRef]
64. Altschuler, E.; Pignotti, A. Nonlinear Model of Flaw Detection in Steel Pipes by Magnetic Flux Leakage. NDT E Int. 1995, 28, 35–40. [CrossRef]
65. Sun, Y.; Feng, B.; Ye, Z.; Liu, S.; Li, D.; Kang, Y.; Gu, M.; Liu, C. Change Trends of Magnetic Flux Leakage with Increasing Magnetic Excitation. Insight Non-Destr. Test. Cond. Monit. 2015, 57, 689–696. [CrossRef]
66. Sun, Y.; Kang, Y. Magnetic Compression Effect in Present MFL Testing Sensor. Sens.

Actuators A Phys. 2010, 160, 54–59. [CrossRef]
67. Sun, Y.; Kang, Y. A New MFL Principle and Method Based on Near-Zero Background Magnetic Field. NDT E Int. 2010, 43, 348–353. [CrossRef]
68. Katoh, M.; Nishio, K.; Yamaguchi, T. The Influence of Modeled B-H Curve on the Density of the Magnetic Leakage Flux Due to a Flaw Using Yoke-Magnetization. NDT E Int. 2004, 37, 603–609. [CrossRef]
69. Park, G.S.; Park, S.H. Analysis of the Velocity-Induced Eddy Current in MFL Type NDT. IEEE Trans. Magn. 2004, 40, 663–666. [CrossRef]
70. Li, Y.; Tian, G.Y.; Ward, S. Numerical Simulation on Magnetic Flux Leakage Evaluation at High Speed. NDT E Int. 2006, 39, 367–373. [CrossRef]
71. Antipov, A.G.; Markov, A.A. 3D Simulation and Experiment on High Speed Rail MFL Inspection. NDT E Int. 2018, 98, 177–185. [CrossRef]
72. Shin, Y. Numerical Prediction of Operating Conditions for Magnetic Flux Leakage Inspection of Moving Steel Sheets. IEEE Trans. Magn. 1997, 33, 2127–2130. [CrossRef]
73. Feng, B.; Deng, K.; Wang, S.; Chen, S.; Kang, Y. Theoretical Analysis on the Distribution of Eddy Current in Motion-Induced Eddy Current Testing and High-Speed MFL Testing. J. Nondestruct. Eval. 2022, 41, 59. [CrossRef]
74. Du, Z.; Ruan, J.; Peng, Y.; Yu, S.; Zhang, Y.; Gan, Y.; Li, T. 3-D FEM Simulation of Velocity Effects on Magnetic Flux Leakage Testing Signals. IEEE Trans. Magn. 2008, 44, 1642–1645. [CrossRef]
75. Feng, B.; Kang, Y.; Sun, Y.; Yang, Y.; Yan, X. Influence of Motion Induced Eddy Current on the Magnetization of Steel Pipe and MFL Signal. Int. J. Appl. Electromagn. Mech. 2016, 52, 357–362. [CrossRef]
76. Wu, J.; Xia, H.; Feng, B.; Li, E.; Huang, X.; Kang, Y. The Effect of Motion-Induced Eddy Current on Circumferential Magnetization in MFL Testing for a Steel Pipe. IEEE Trans. Magn. 2017, 53, 6201506. [CrossRef]
77. Katragadda, G.; Lord, W.; Sun, Y.S.; Udpa, S.; Udpa, L. Alternative Magnetic Flux Leakage Modalities for Pipeline Inspection. IEEE Trans. Magn. 1996, 32, 1581–1584. [CrossRef]
78. Wang, P.; Gao, Y.; Tian, G.; Wang, H. Velocity Effect Analysis of Dynamic Magnetization in High Speed Magnetic Flux Leakage Inspection. NDT E Int. 2014, 64, 7–12. [CrossRef]
79. Pullen, A.L.; Charlton, P.C.; Pearson, N.R.; Whitehead, N.J. Practical Evaluation of Velocity Effects on the Magnetic Flux Leakage Technique for Storage Tank Inspection. Insight 2020, 62, 73–80. [CrossRef]
80. Pullen, A.L.; Charlton, P.C.; Pearson, N.R.; Whitehead, N.J. Magnetic Flux Leakage Scanning Velocities for Tank Floor Inspection. IEEE Trans. Magn. 2018, 54, 1–8. [CrossRef]
81. Zhang, L.; Belblidia, F.; Cameron, I.; Sienz, J.; Boat, M.; Pearson, N. Influence of Specimen Velocity on the Leakage Signal in Magnetic Flux Leakage Type Nondestructive Testing. J. Nondestruct. Eval. 2015, 34, 6. [CrossRef]
82. Usarek, Z.; Chmielewski, M.; Piotrowski, L. Reduction of the Velocity Impact on the Magnetic Flux Leakage Signal. J. Nondestruct. Eval. 2019, 38, 28. [CrossRef]
83. Antipov, A.G.; Markov, A.A. Using a Tail Field in High-Speed Magnetic Flux Leakage Testing. J. Nondestruct. Eval. 2022, 41, 1–9. [CrossRef]
84. Feng, B.; Kang, Y.; Sun, Y. Theoretical Analysis and Numerical Simulation of the Feasibility of Inspecting Nonferromagnetic Conductors by an MFL Testing Apparatus. Res. Nondestruct. Eval. 2016, 27, 100–111. [CrossRef]
85. Yuan, F.; Yu, Y.; Li, L.; Tian, G. Investigation of DC Electromagnetic-Based Motion Induced Eddy Current on NDT for Crack Detection. IEEE Sens. J. 2021, 21, 7449–7457. [CrossRef]

86. Uhlig, R.P.; Zec, M.; Brauer, H.; Thess, A. Lorentz Force Eddy Current Testing: A Prototype Model. J. Nondestruct. Eval. 2012, 31, 357–372. [CrossRef]
87. Carlstedt, M.; Porzig, K.; Uhlig, R.P.; Zec, M.; Ziolkowski, M.; Brauer, H. Application of Lorentz Force Eddy Current Testing and Eddy Current Testing on Moving Nonmagnetic Conductors. Int. J. Appl. Electromagn. Mech. 2014, 45, 519–526. [CrossRef]
88. Kasai, N.; Sekine, K.; Maruyama, H. Influence of Corrosion Products on Magnetic Flux Leakage Signals in Inspection of Far-Side Metal-Loss Defects in Oil Storage Tank Bottom Floors. J. Japan Pet. Inst. 2004, 47, 19–26. [CrossRef]
89. Long, Y.; Huang, S.; Peng, L.; Wang, S.; Zhao, W. A Novel Compensation Method of Probe Gesture for Magnetic Flux Leakage Testing. IEEE Sens. J. 2021, 21, 10854–10863. [CrossRef] 90. Wang, Y.; Melikhov, Y.; Meydan, T.; Yang, Z.; Wu, D.; Wu, B.; He, C.; Liu, X. Stress-Dependent Magnetic Flux Leakage: Finite Element Modelling Simulations Versus Experiments. J. Nondestruct. Eval. 2020, 39, 1–9. [CrossRef]
91. Mandal, K.; Corey, A.; Loukas, M.E.; Weyman, P.; Eichenberger, J.; Atherton, D.L. The Effects of Defect Depth and Bending Stress on Magnetic Barkhausen Noise and Flux-Leakage Signals. J. Phys. D Appl. Phys. 1997, 30, 1976–1983. [CrossRef]
92. Wang, Y.; Liu, X.; Wu, B.; Xiao, J.; Wu, D.; He, C. Dipole Modeling of Stress-Dependent Magnetic Flux Leakage. NDT E Int. 2018, 95, 1–8. [CrossRef]
93. Gao, G.; Lian, M.; Xu, Y.; Qin, Y.; Gao, L. The Effect of Variable Tensile Stress on the MFL Signal Response of Defective Wire Ropes. Insight Non-Destr. Test. Cond. Monit. 2016, 58, 135–141. [CrossRef]
94. Shi, P.; Bai, P.; Chen, H.E.; Su, S.; Chen, Z. The Magneto-Elastoplastic Coupling Effect on the Magnetic Flux Leakage Signal. J. Magn. Magn. Mater. 2020, 504, 166669. [CrossRef]
95. Babbar, V.; Shiari, B.; Clapham, L. Mechanical Damage Detection With Magnetic Flux Leakage Tools: Modeling the Effect of Localized Residual Stresses. IEEE Trans. Magn. 2004, 40, 43–49. [CrossRef]
96. Deng, Z.; Sun, Y.; Yang, Y.; Kang, Y. Effects of Surface Roughness on Magnetic Flux Leakage Testing of Micro-Cracks. Meas. Sci. Technol. 2017, 28, 045003. [CrossRef]
97. Yang, Y.; Li, L.; Deng, Z.; Kang, Y. Theoretical Analysis and Simulation of a New SNR Improvement Method for the Rough Surface Crack in MFL Detection. Int. J. Appl. Electromagn. Mech. 2016, 52, 1401–1408. [CrossRef]
[98] Rao, B.P.C.; Thirunavukkarasu, S.; Nand, K.K.; Jayakumar, T.; Kalyanasundaram, P.; Raj, B. Enhancement of Magnetic Flux Leakage Images of Defects in Carbon Steel Using Eigen Vector Based Approach. Nondestruct. Test. Eval. 2008, 23, 35–42. [CrossRef]
[99] Li, E.; Wang, J.; Wu, J.; Kang, Y. Spatial-Spectrum-Based Measurement of the Surface Roughness of Ferromagnetic Components Using Magnetic Flux Leakage Method. IEEE Trans. Instrum. Meas. 2021, 70, 1–10. [CrossRef]
[100] Brondel, D.; Edwards, R.; Hayman, A.; Hill, D.; Mehta, S.; Semerad, T. Corrosion in the oil industry.Oilfield Rev. 1994, 6, 4–18

[101] API (American Petroleum Institute). API Spec 5D-Specification for Drill Pipe, 5th ed.; API: Washington, DC,USA, 2002.

[102] Sun, Y.; Kang, Y. Magnetic mechanisms of magnetic flux leakage nondestructive testing. Appl. Phys. Lett. 2013, 103, 184104.

[103] Ramuhalli, P.; Udpa, L.; Udpa, S.S. Neural network-based inversion algorithms in magnetic flux leakage nondestructive evaluation. J. Appl. Phys. 2003, 93, 8274–8276

[104] Sun, Y.; Kang, Y. A new MFL principle and method based on near-zero background

magnetic field. NDT E Int. 2010, 43, 348–353

[105] Tian, G.Y.; Wilson, J.; Morozov, M.; Thompson, D.O.; Chimenti, D.E. Complementary electromagnetic non-destructive evaluation. AIP Conf. Proc. 2011, 1335, 1256.

[106] Zhiye, D.; Jiangjun, R.; Ying, P.; Shifeng, Y.; Yu, Z.; Yan, G.; Tianwei, L. 3-D FEM simulation of velocity effects on magnetic flux leakage testing signals. IEEE Trans. Magn. 2008, 44, 1642–1645.

[107] Shin, Y.K.; Lord, W. Numerical modeling of moving probe effects for electromagnetic nondestructive evaluation. IEEE Trans. Magn. 1993, 29, 1865–1868.

[108] Lu, S.; Feng, J.; Li, F.; Liu, J. Precise Inversion for the Reconstruction of Arbitrary Defect Profiles Considering Velocity Effect in Magnetic Flux Leakage Testing. IEEE Trans. Magn. 2017, 53, 1–12